THE FLORIDA STATE UNIVERSITY

COLLEGE OF ARTS AND SCIENCES

THE EFFECTS OF THE HORIZONTAL RESOLUTION OF THE SEA SURFACE TEMPERATURE FIELD ON THE FSU SPECTRAL MODEL

By

BRENT D. HICKEL

A Thesis submitted to the
Department of Meteorology
in partial fulfillment of the requirements
for the degree of Master of Science

Degree Awarded:
Fall Semester, 1994

Fall Semester, 1994

The members of the Committee approve the thesis of Brent D. Hickel defended on August 4, 1994.

James J. O'Brien
Professor Directing Thesis

T. N. Krishnamurti
Committee Member

Eric A. Smith
Committee Member

Acknowledgment

This work was supported by the Air Force Institute of Technology and the Department of Defense High Performance Computing Program.

I wish to thank Dr. Darlene Oosterhof for her patience and assistance with the FSU spectral model, Mark Verschell for his help in preparing the data and with the computer graphics, and my friends at the Mesoscale Air-Sea Interaction Group for their support during my studies.

Finally, I wish to thank Dr. James O'Brien for running a first-class research group and for guiding me through my graduate studies and research.

Table of Contents

List of Figures

case A near wavenumber 36 above which a 5° by 5° SST field would have no variance.

Freda, Holly (west to east). Of interest is the merging of Holly and Freda at hour 72-96 and the intensification of the merged storm.

Abstract

This study examines the effects of higher wavenumbers in the boundary forcing sea surface temperature (SST) on the forecast of an atmospheric model. The model is the FSU global spectral model employing the triangular truncation method at 170 wavenumbers for a horizontal resolution of .7° lattitude by .7° longitude. The boundary forcing is provided by a fine scale SST, a smoothed version of the same SST with the higher wavenumbers removed, and a combination field where a region off Japan bounded by 20° N to 55° N by 120° E to 150° E from the fine scale SST is patched into the smoothed SST field.

The results indicate that inclusion of higher wavenumbers in the boundary forcing SST significantly impacts the behavior of the atmospheric model. The areas downstream from regions of strong spatial gradient in the SST field, such as the Kuroshio and Gulf Stream have the largest differences. Geopotential height differences at 500 mb between the fine and smoothed SST model runs are as high as 230 meters south of Japan by day 5 of the forecast period. Pacific typhoon intensity is better modeled using the high resolution SST. The effects from the boundary forcing are minor for short term weather forecasting, but become increasingly important as the forecast period increases. The effects of the initial atmospheric conditions are tested and are clearly smaller than the impact of the fine scale SST.

period increases. The effects of the initial atmospheric conditions are tested and are clearly smaller than the impact of the fine scale SST.

It is conjectured that medium range, 5-14 day weather forecasts will be greatly improved if the best resolution observed SST is used as an ocean forcing condition. We conclude that coupled ocean-atmosphere models will be negatively impacted if a low resolution ocean model is coupled to a higher resolution atmospheric model.

CHAPTER 1

INTRODUCTION

Researchers have steadily increased the horizontal and vertical resolution of atmospheric, oceanic and coupled models as computer power has increased. Numerous studies by researchers such as Mo et al. (1994), Gleckler and Taylor (1993), and Von Storch et al. (1993) have examined the impact of resolution on model output. Typically these studies run an atmospheric general circulation model at spectral resolutions of T21, T42, T63, and T106 or a coupled ocean-atmosphere model at T21 and T42, then compare the output from the model runs. Gleckler and Taylor found that locally large differences among the higher resolution runs suggest that convergence may not be achieved even at T106. Trenberth and Solomon (1993) examined the spectra of various atmospheric variables and concluded that in the lower troposphere there is more power in the higher wavenumbers than in the upper troposphere due to the proximity to the lower boundary. This study examines the effect of higher wavenumbers in the lower boundary sea surface temperature (SST) field on the output from a global atmospheric model. We use a high resolution SST and a filtered version of the same SST, with the higher wavenumbers removed, as the boundary forcing to the model.

Historically, the SST data used in operational forecast models have boundary forcing to the model.

Historically, the SST data used in operational forecast models have improved as model resolution has increased and as advancements in

remote sensing techniques have improved global data coverage. Model resolution at the major forecast centers has increased from T42 in the early 1980s to as high as T126 currently (e.g., Kanamitsu et al. 1991, Petersen et al. 1991). The SST data provided by National Meteorological Center (NMC) have steadily improved from a blending of ship and buoy data available at 5° by 5° degrees in the early 1980s, to 1° by 1° data today. The period over which the data are collected to form the SST data sets has shrunk from climatological time scales to weekly data that are currently updated daily (e.g., Reynolds 1985, 1988, 1991, 1994).

This study differs significantly from other studies on the effects of model resolution in several ways. The model resolution is held constant at T170. The model is integrated for 6 days compared to several years or longer for a typical climatological model integration. Also, the SST used in a majority of the studies are climatology or the output from an ocean model. We've chosen to use the observed fine scale SST field as the lower boundary to provide the most realistic forcing at the lower boundary. However, we expect that certain aspects of our results will be applicable to climate and coupled modeling as well as to short and medium range modeling.

In the following pages, we first describe the model along with a brief description of how it has been used in past studies. Next, we discuss the data used in the model and the reason for choosing this data set. The experiment design section describes how we've used the data to force the model in each of four cases. Case A is forced with the highest resolution SST. Case B is forced with a smooth version of the SST. Case C has a fine model in each of four cases. Case A is forced with the highest resolution SST. Case B is forced with a smooth version of the SST. Case C has a fine scale SST only in the region of the Kuroshio. Case D uses the same SST as

Case A with different initial conditions. In the results section, the differences in the output from the Case A and Case B model runs are presented along with the results from Cases C and D, which were designed to test the validity of the experiment. Finally, we discuss the implications of the results and how they might be used in other studies. We show that by including the higher wavenumbers in the SST boundary forcing the model forecast is changed among the four model runs, especially downstream from regions of high spatial gradients in the SST field.

CHAPTER 2

MODEL

The Florida State University (FSU) spectral model is a high-resolution global spectral model based on the spectral transform method. The model has been used in numerous studies including Krishnamurti et al. (1993), where a complex triple typhoon scenario over the Western Pacific was modeled at a spectral truncation of 106 wavenumbers. This study involved examining the model response to changes in the physical initialization. Two model integrations were performed with the same atmospheric conditions used to initialize the model atmosphere, but in the second case the vorticity, divergence and surface pressure fields were nudged by incorporating "observed rainfall rates" in the initialization procedure. All three of the typhoons formed and developed in the nudged case, but in the control case the two easternmost storms merged into an area of weak low pressure. Here, we've chosen to model the same time period: 6-12 September 1987, with the atmospheric resolution increased to 170 wavenumbers without including the "observed rainfall rates." Thus, our results should be similar to the control experiment by Krishnamurti et al. in the typhoon region. The following is an outline of the global model taken from Krishnamurti et al. (1994) where the model was used to examine Hurricane Frederic, 1979 at T170 resolution:
taken from Krishnamurti et al. (1994) where the model was used to examine Hurricane Frederic, 1979 at T170 resolution:

(a) Independent variables: x, y, σ, t.

(b) Dependent variables: vorticity, divergence, surface pressure, vertical velocity, temperature and humidity.

(c) Horizontal resolution: triangular 170 waves.

(d) Vertical resolution: 15 layers between roughly 50 and 1000 mb.

(e) Semi-implicit time differencing scheme.

(f) Envelope orography (Wallace et al., 1983).

(g) Central differences in the vertical for all variables except humidity, which is handled by an upstream differencing scheme.

(h) Fourth-order horizontal diffusion (Kanamitsu et al., 1983).

(i) Kuo-type cumulus parameterization (Krishnamurti et al., 1983).

(j) Shallow convection (Tiedke, 1984).

(k) Dry convective adjustment.

(l) Large scale condensation (Kanamitsu, 1975).

(m) Surface fluxes by means of similarity theory (Businger et al., 1971).

(n) Vertical distribution of fluxes using diffusive formulation where the exchange coefficients are functions of the Richardson number (Louis, 1979).

(o) Longwave and shortwave radiative fluxes based on a band model, (Harshvardan and Corsetti, 1984; Lacis and Hansen, 1974).

(p) Diurnal cycle.

(q) Parameterization of low, middle and high clouds based on threshold relative humidity for radiative transfer calculations.

(r) Surface energy balance coupled to the similarity theory (Krishnamurti et al., 1991).

(r) Surface energy balance coupled to the similarity theory (Krishnamurti et al., 1991).

(s) Nonlinear normal mode initialization - five vertical modes (Kitade, 1983).

(t) Physical initialization (Krishnamurti et al., 1991).

Our study used the model for four different cases, which would require about 72 hours of Cray YMP computer time per case. The first two cases are integrated for 6 days, from 6 September 1987 at 00Z out to the 12th at 00Z. Due to the intensive computational needs of the atmospheric model, Cases C and D are only run out to 8 September at 00Z. The first three cases involve integrating the model starting with atmospheric data from 6 September 1987 at 00Z, whereas the fourth case was started with atmospheric data from 5 September 1987 at 12Z. The differences in the SST data used and the different starting times in the four studies are described in the following two sections.

CHAPTER 3

DATA

Currently, global SST data is available from a variety of sources, including NMC, the University of Miami/Rosenstiel School of Marine and Atmospheric Science (e.g., Smith 1992) and the COADS monthly data set. We've chosen to use the Rosenstiel data set because we desire that the SST data resolution be at least as high as that of our atmospheric model. The Rosenstiel data is from the NOAA very high resolution radiometer multichannel sea surface temperature data set and is available at a resolution of about .176° by .176° or 18 km at the equator. This represents a weekly average of the data available at each grid point. The comparatively long time scales for changes in SST, as discussed by Reynolds (1978) compared to atmospheric time scales allow us to hold the SST constant for the 6 days of the model run. This data does not blend in ship and buoy data as in the NMC data described by Reynolds (1994) and the statistics have not been cleaned up using the optimal interpolation methods used in creating the NMC data set. However, this study is not looking at forecast statistics, thus the data and the model are treated as if they are perfect and differences in the model output are attributed to the differences in the boundary forcing used in each case.

differences in the boundary forcing used in each case.

The Miami/Rosenstiel SST data are interpolated to the model resolution using a cubic spline interpolation for use in Cases A and D. The data for Case B was prepared by filtering the Case A data with a fourth-order Butterworth filter to effectively eliminate the variance in wavenumbers higher than 36. The cutoff wavenumber was chosen so that the data would have the spectrum of a 5° by 5° data field. Figures 3-1 and 3-2 show a region of the fine and smooth resolution SST fields. The difference in resolution between the two data fields is readily seen. Figure 3-3 demonstrates the how much of the total variance in the Rosenstiel data spectrum would be present for some common model resolution. For example, truncating the spectrum at 21 wavenumbers would account for only about 65% of the total variance in the data spectrum.

The filtering characteristics of the Butterworth filter are demonstrated in Figure 3-4, where the spectrum of the filtered data divided by the spectrum of the fine scale data is shown. The filtered data set loses about 27% of the global spatial variance of the original data due to the elimination of the higher wavenumbers. We also examined the spectrum of the September 1987 COADS SST data set and found that it accounts for only about 60% of the variance of the Rosensteil SST. This would poorly represent the spectral characteristics of the Rosensteil SST for the first week in September of 1987. Thus, a study using September COADS data as an experimental case could not be readily interpreted as important spectral details of the SST spectrum are missing due to the data resolution of 2° by 2 and the month of data used to prepare the data set.

resolution of 2° by 2 and the month of data used to prepare the data set.

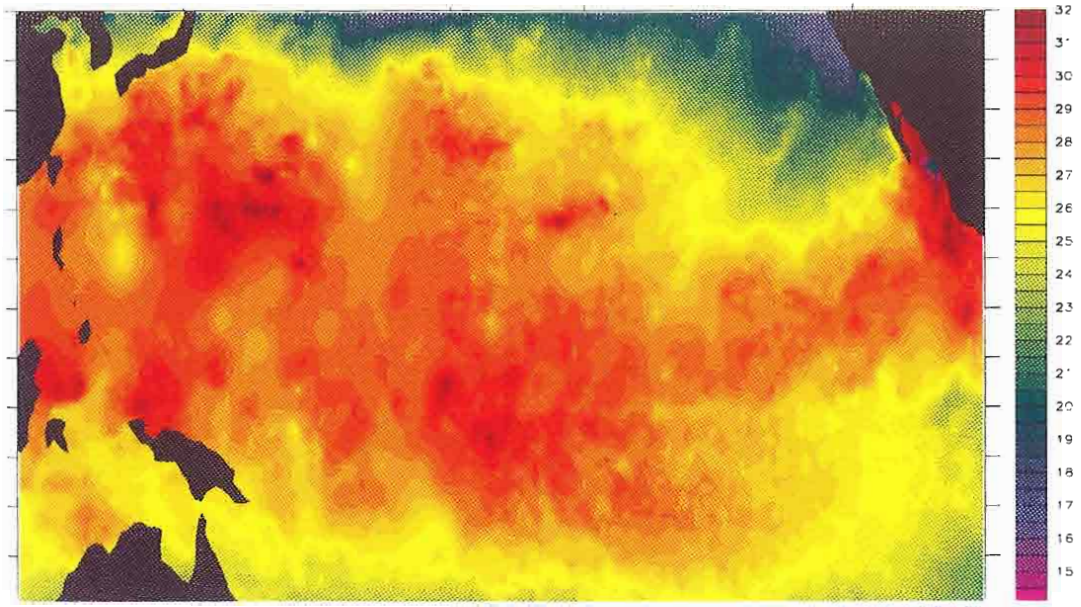

Fig. 3-1: A region of the sea surface temperature field used in Case A (°Celsius).

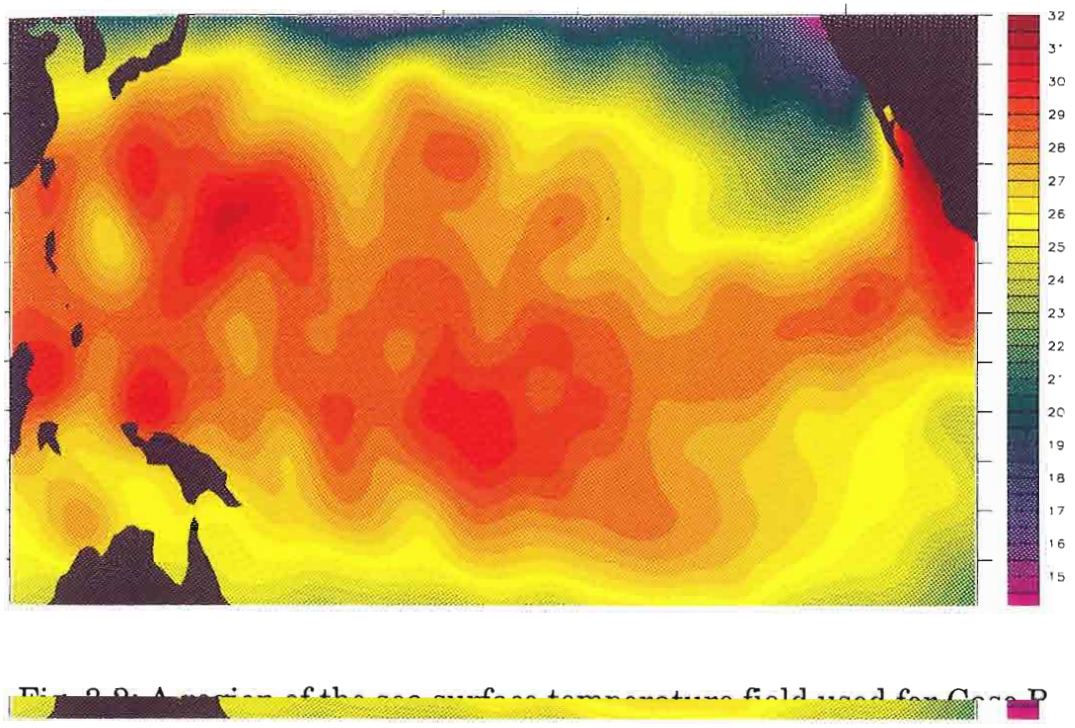

Fig. 3-2: A region of the sea surface temperature field used for Case B (°Celsius).

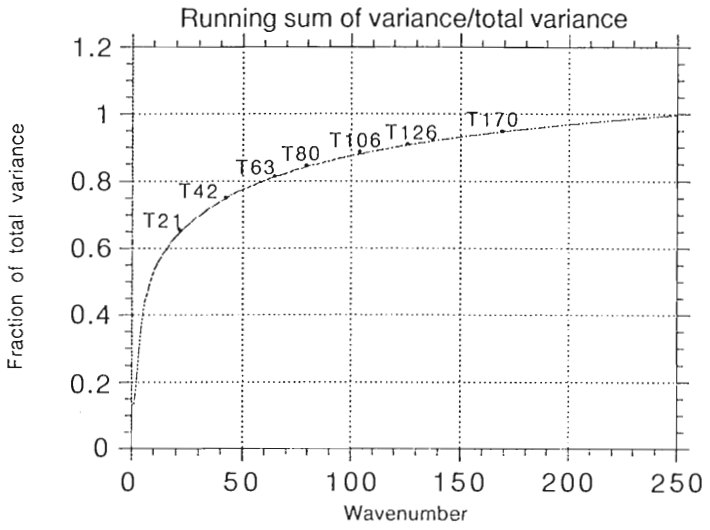

Fig. 3-3: Running sum of the variance divided by the total variance in the fine scale SST versus wavenumber. Common model resolutions are included for reference.

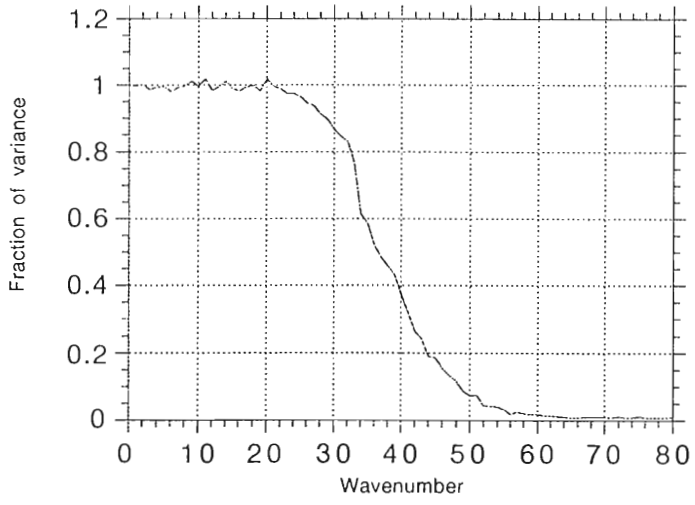

Fig. 3-4: Variance at each wavenumber in Case B divided by the variance at each wavenumber in Case A

Fig. 3-4: Variance at each wavenumber in Case B divided by the variance at each wavenumber in Case A.

In Case C a region of the fine scale SST field covering the Kuroshio (20° N to 60° N by 110° E to 150° E) is patched into the smoothed SST field to form a third SST field. The boundaries of the patch were smoothed to remove discontinuities. The region of the patch accounts for about 35% of the variance in the higher wavenumbers of the fine scale SST spectrum over the latitudes of the patch. This is depicted in Figure 3-5.
The residual variance in the higher wavenumbers from the smoothed SST field has been removed to yield only the variance associated with the patch.

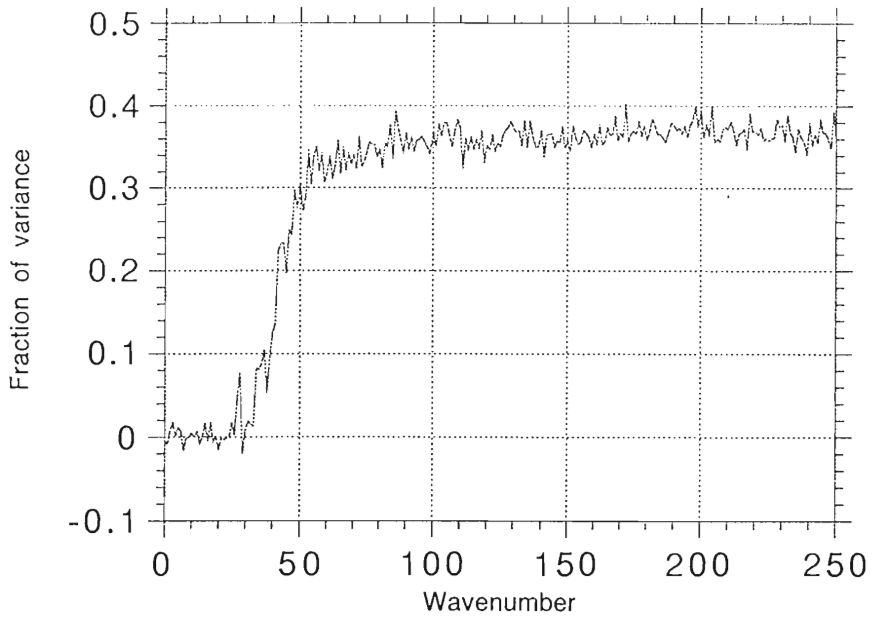

Fig. 3-5: Variance at each wavenumber for the latitudes of the patch

Fig. 3-5: Variance at each wavenumber for the latitudes of the patch region of Case C minus the Case B variance, then divided by the variance in each wavenumber from Case A at those latitudes.

It is important to recognize that by using the high resolution SST field to prepare the SST input fields for all model runs any biases to the SST retrieval methods are present in each model run. Thus, the data, interpolated to the resolution required for each of our model runs, will contain information at wavenumbers as high as needed for each of the cases in this experiment.

CHAPTER 4

EXPERIMENT DESIGN

Four model runs, which are referred to as Cases A, B, C, D, are calculated using the FSU atmospheric spectral model to show the effects of systematic perturbations to the boundary forcing on the model output. The first three cases are started with the initial atmospheric data from 6 September 1987 at 00Z, whereas Case D is started with the atmospheric data from 5 September 1987 at 12Z. Model run A is the control forecast using the high resolution SST data set as the boundary forcing. It is regarded as truth. This provides a basis for comparison with model runs B, C, and D. Model run B uses the smoothed SST field where the variance associated with wavenumbers higher than 36 has been filtered out. Model run C uses the smoothed SST field except in a region off Japan bounded by 20° N to 55° N by 120° E to 150° E from the high resolution SST field was patched into the smoothed SST field.

The comparison between model runs A and B is designed to demonstrate how the output from the model would differ when the high wavenumbers are present versus when they have been removed from the boundary forcing. Namias (1974) suggests that areas of high SST gradient will provide an enhanced source of atmospheric baroclinicity. Our hypothesis is that the removal of the higher wavenumbers in Case B will

will provide an enhanced source of atmospheric baroclinicity. Our

hypothesis is that the removal of the higher wavenumbers in Case B will result in considerable differences in the models' output, especially

downstream from regions of high gradient in the SST fields. This simulates a coupled ocean-atmosphere model where the atmospheric model is run at a much higher resolution than the oceanic model. It is also useful in demonstrating the effects on the output from a high resolution forecast model when a lower resolution SST field is used as the lower boundary condition. Commonly, in research using high resolution atmospheric models, the SST fields are interpolated from lower resolution data fields to the model resolution. This interpolation does not properly include the high wavenumber contributions of the true SST field. This comparison can also be extended to climate model runs such as Gleckler and Taylor (1993), where monthly climatological data are interpolated spatially to the resolution of the model run and then interpolated temporally to a desired time interval, say each week of the year. These data are then inserted as the model run progresses for periods as long as several centuries.

Case C is designed to demonstrate how a particular region of high SST gradient, the Kuroshio, effects the output of the model. The Kuroshio was chosen because a strong weather system, the triple typhoon, was present over this region, whereas no strong weather system develops over the Gulf Stream during the period of the model integration. Comparison with model runs A and B should give some insight into the effects of the Kuroshio region on the response of a numerical model and allow some conjecture as to the effects of other domains such as the Gulf Stream on the atmospheric response. With about 35% of the total variance in the higher wavenumbers accounted for by the patch, we expect the model to behave similarily to Case A over and downstream from the patch region.

higher wavenumbers accounted for by the patch, we expect the model to behave similarily to Case A over and downstream from the patch region.

Case D is run to show how the model responds to changes in the initial state of the atmosphere. Case D is started with the atmospheric conditions from 5/12Z and run out to 8 September at 00Z. Our conjecture is that Case D and Case A should yield almost similar results when compared with Case B. This would verify that the differences in results between Case A and Case B are due to the difference in boundary forcing and not due to nonlinear response of the model to the initial state of the atmosphere.

Comparison between the model output from the four cases is made at the 500 mb level downstream from two areas of high SST gradient; the Kuroshio and the Gulf Stream. The week of September 6 was interesting in that a triple typhoon formed in the Western Pacific Ocean. We will look at the intensities and movement of the storms in the output from Cases A and B. Comparison is made with Krishnamurti et al. (1993) in the typhoon region to interpret the atmospheric response.

CHAPTER 5

RESULTS

The output data available from the atmospheric model includes geopotential height, temperature, U and V components of wind, specific humidity, divergence, vertical velocity, and vorticity at the 100, 200, 300, 400, 500, 700, 850 and 1000 mb pressure levels along with sea surface temperature, precipitation and sea level pressure (SLP). Out of this vast amount of information the SLP and the 500 mb geopotential heights are selected to examine the four cases. The global coverage of the model provides a large area over which the output data can be studied. We've chosen to concentrate on the SLP and the 500 mb geopotential height differences over the typhoon region for comparison with Krishnamurti et al. and the 500 mb geopotential height differences downstream from the two strongest western boundary currents: the Kuroshio and the Gulf Stream. The phase characteristics of the Case A and Case B model integrations will be examined by comparing the 500 mb height fields. The 500 mb geopotential height differences were used to simplify our understanding of the differences among the four model runs. First, we will discuss the 500 mb geopotential height differences between cases A and B over the Northern Pacific, then the Northern Atlantic. Next, we will cover the region of the typhoons using the SLP and 500 mb geopotential height

over the Northern Pacific, then the Northern Atlantic. Next, we will cover the region of the typhoons using the SLP and 500 mb geopotential height

differences. Finally, we will discuss the 500 mb geopotential height

differences for cases A and B versus cases C and D over the Northern Pacific and the Northern Atlantic and discuss the difference fields.

Figure 5-1 illustrates the 500 mb geopotential height difference field between Cases A and B over the North Pacific as it evolves over the 6-day period. The dominant initial features are the higher geopotential height in Case A over Japan and the Rocky Mountains. The geopotential height feature over the Rocky Mountains remains relatively constant during the 6-day period. The dominant features toward the end of the period are the higher geopotential height over Japan, which increases to 150 meters by day 6, the lower geopotential heights feature south of Japan, which marks a typhoon's location and reaches a maximum difference of 250 meters by day 5 and the geopotential height differences over Siberia and Alaska, which exceed 90 meters by day 6. These features are generally over or downstream from the region of high SST gradient comprising the Kuroshio.

Figures 5-2a and 5-2b show the 500 mb height fields after 144 hours of integration for Cases A and B over the Northern Pacific. South of Japan a low pressure feature is evident in fig. 5-2a, but not in 5-2b. The trough east of Japan is stronger in Case B and the high pressure feature east of Japan in Case A is missing. The troughing in the Gulf of Alaska appears to be in phase between the two model runs with the trough better defined over Alaska in Case A. The Trough over the Rocky Mountains is stronger in Case and again in phase with Case A.

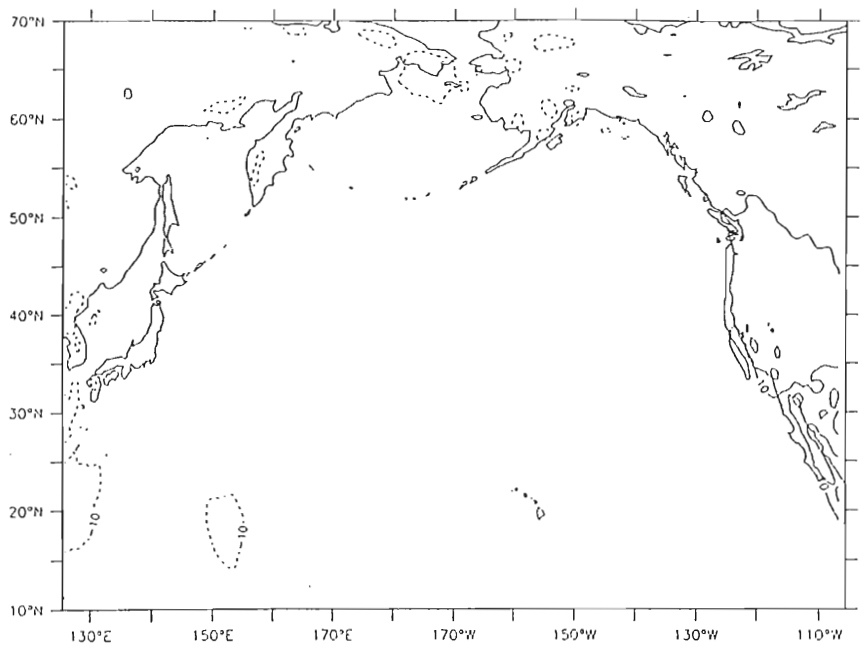

Fig. 5-1a: The 500 mb height differences after 24 hours of integration (7 September at 00Z) between Case A and Case B over the Northern Pacific Ocean (meters).

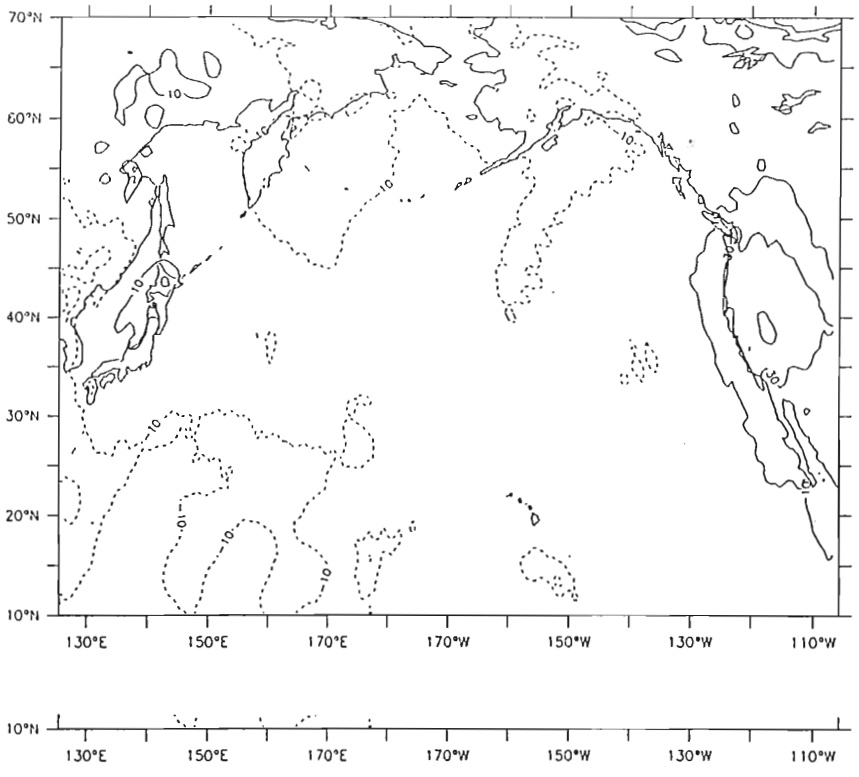

Fig. 5-1b: Same as fig. 5-1a except at 48 hours (8/00Z).

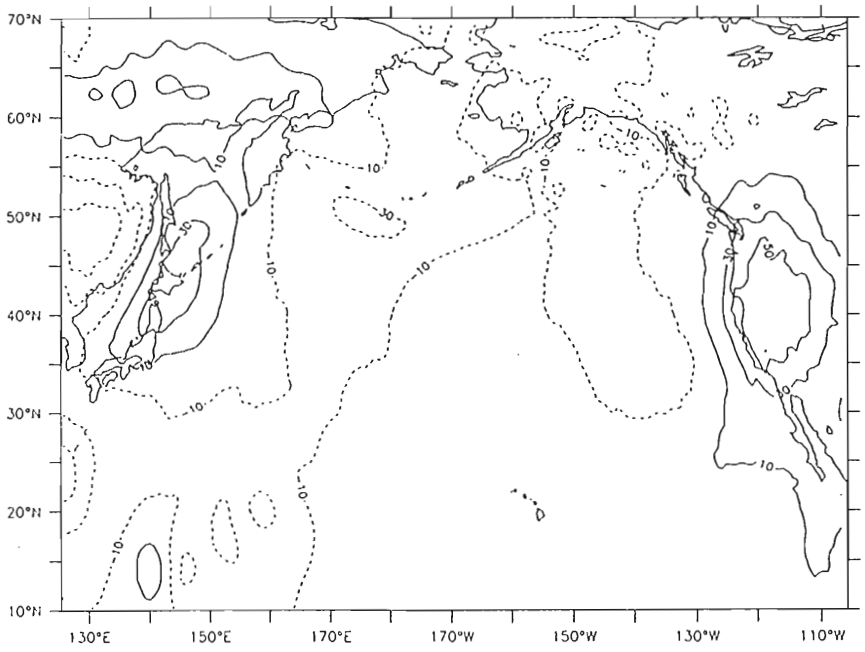

Fig. 5-1c: Same as fig. 5-1a except at 72 hours (9/00Z).

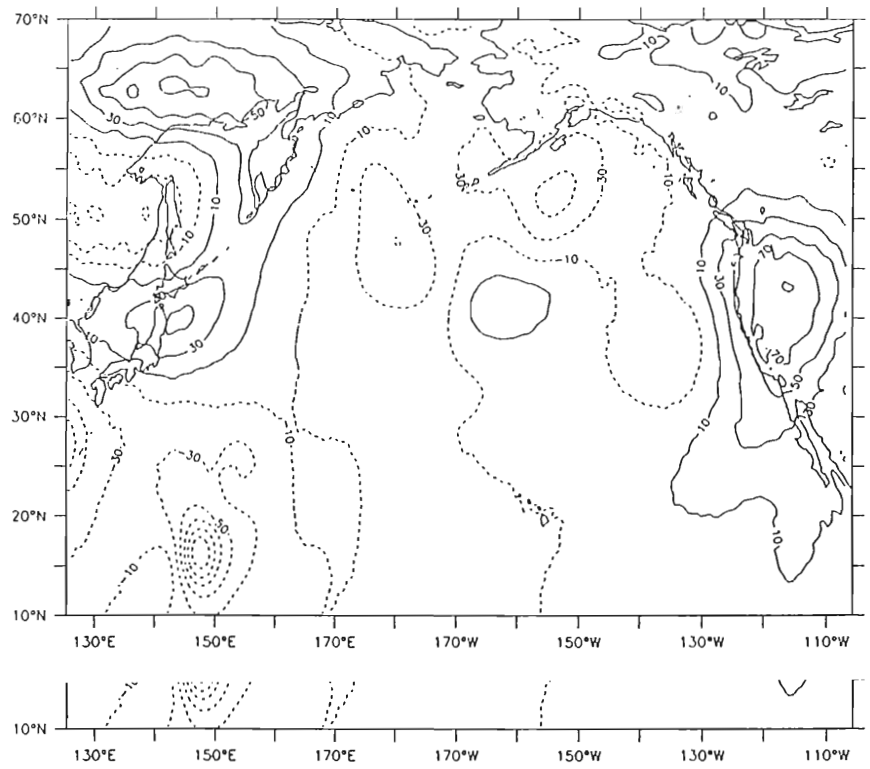

Fig. 5-1d: Same as fig. 5-1a except at 96 hours (10/00Z).

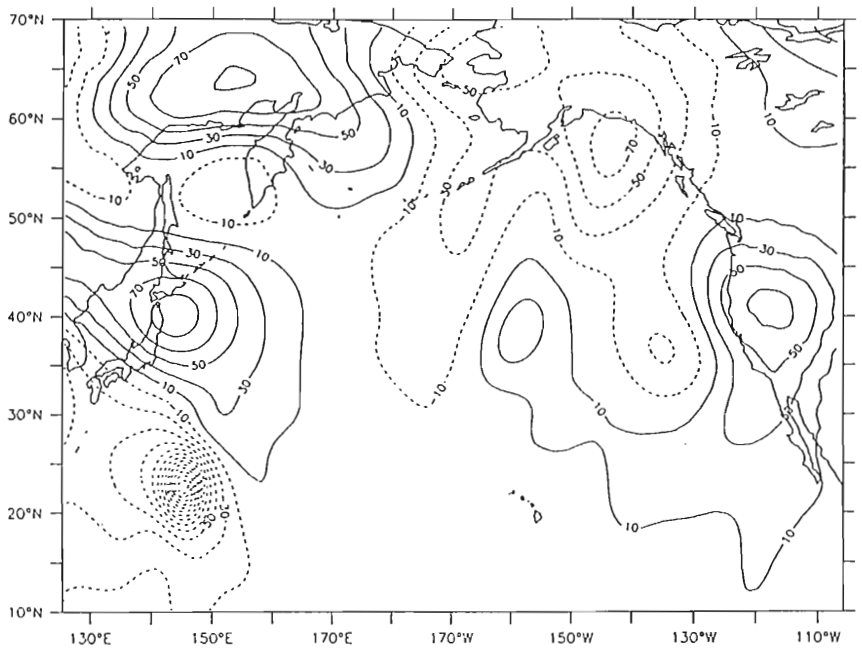

Fig. 5-1e: Same as fig. 5-1a except at 120 hours (11/00Z)..

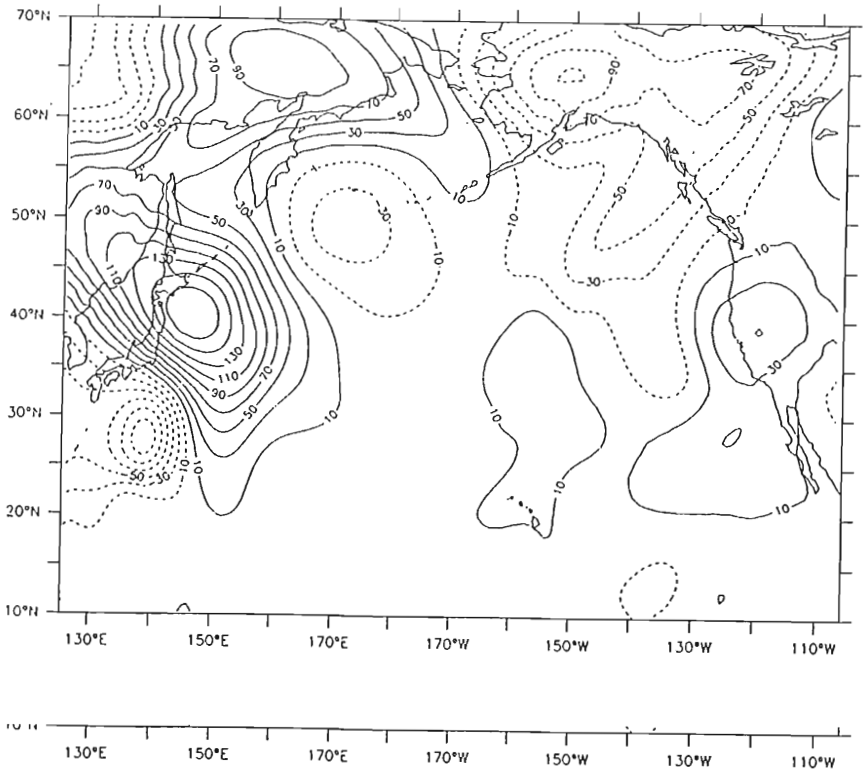

Fig. 5-1f: Same as fig. 5-1a except at 144 hours (12/00Z).

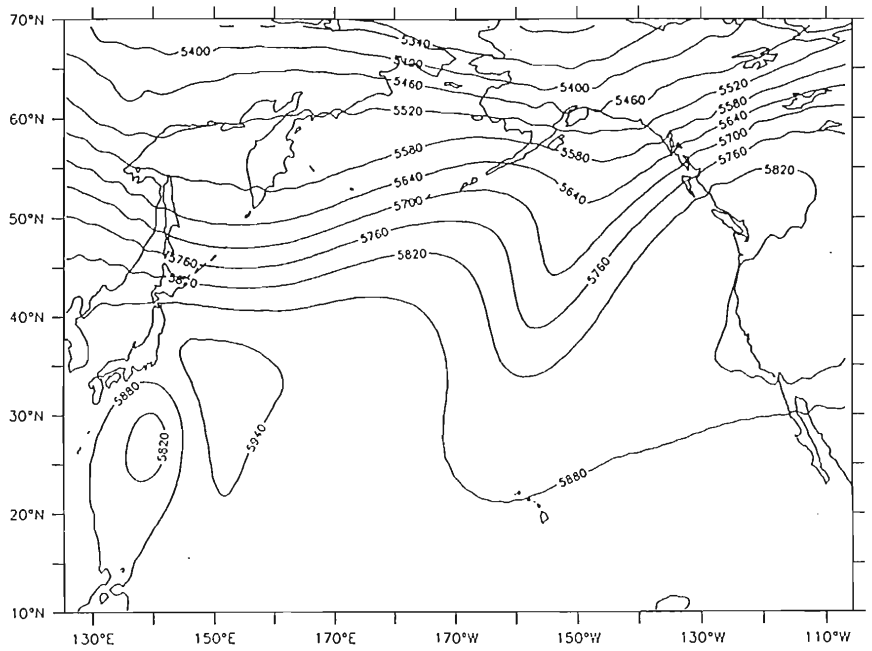

Fig. 5-2a: The 500 mb height contours for Case A at 144 hours (12/00Z) over the Northern Pacific Ocean (meters)

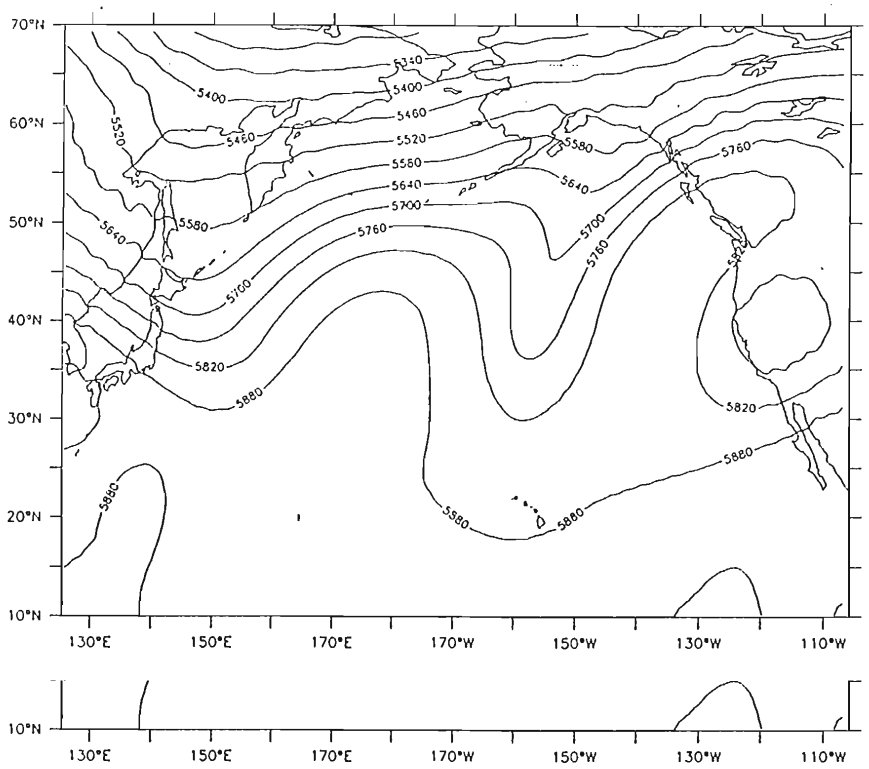

Fig. 5-2b: Same as fig. 5-2a except for Case B.

Figure 5-3 illustrates the evolution of the 500 mb geopotential height difference field between Cases A and B over the North Atlantic during the 6-day period. The dominant initial feature is the 70 meter geopotential height difference over Greenland, which is present until Day 6. The dominant feature that develops is the 110 meter geopotential height difference over the North Atlantic with Case A having the lower geopotential height. A lesser feature is the positive 70 meter geopotential height in Case A over Nova Scotia. These features are directly downstream from the area of high gradient over the Gulf Stream.

Figures 5-4a and 5-4b show the 500 mb height fields after 144 hours of integration for Cases A and B over the Northern Atlantic. Here we see that Case B is slightly ahead of Case A in phase over North America with the trough on the east coast the dominant feature. The ridge over the Hudson Bay is more strongly tilted in Case A and more sharply defined. An important difference is the slight ridging over the Northeast Atlantic in Case B compared with a slight troughing for the region in Case A.

The period of our model runs is especially interesting in that a triple typhoon event occurred, Gerald, Freda and Holly from west to east. This event was studied by Krishnamurti et al. using the FSU spectral model at T106 resolution to compare model runs with and without nudging of the vorticity, divergence and surface pressure fields. The case without nudging resulted in the merging of Freda and Holly. Our model runs were without nudging and concur with the results of Krishnamurti et al. in that our two easternmost typhoons merged by during the model integrations.

our two easternmost typhoons merged by during the model integrations.

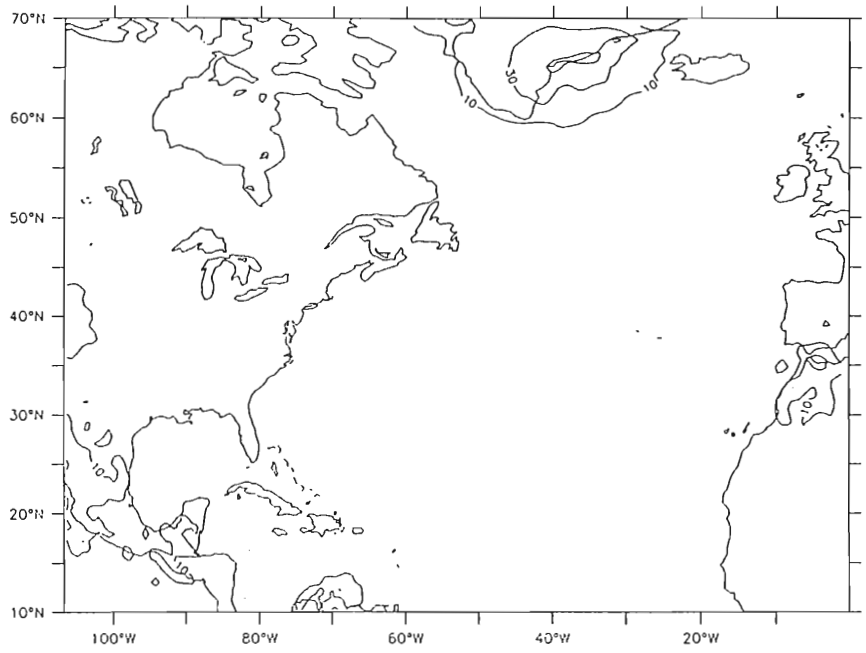

Fig. 5-3a: The 500 mb height differences after 24 hours of integration (7 September at 00Z) between Case A and Case B over the Northern Atlantic Ocean (meters).

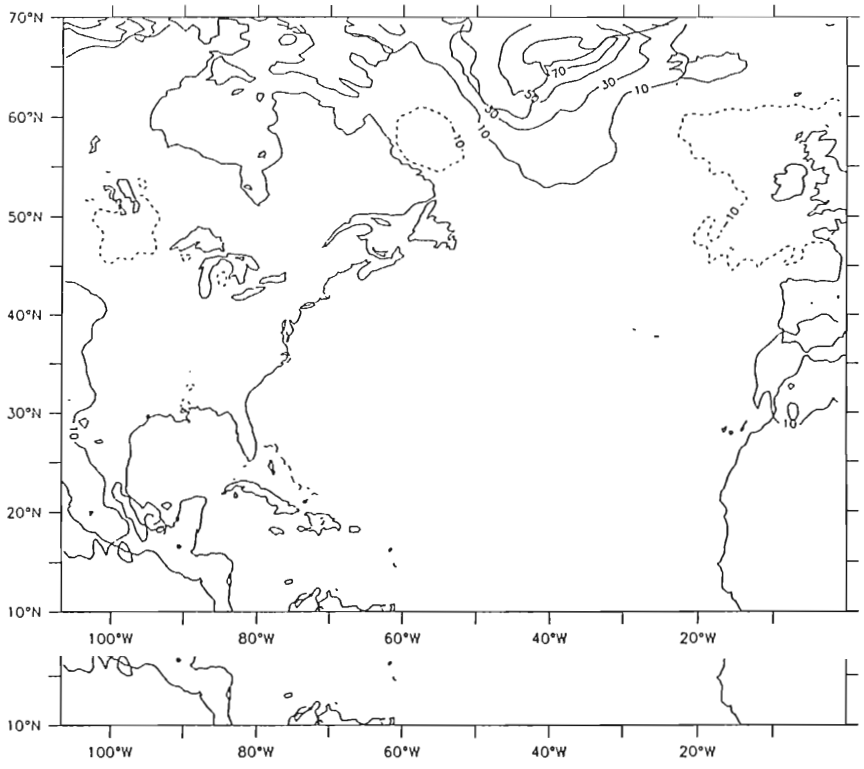

Fig. 5-3b: Same as fig. 5-3a except at 48 hours (8/00Z).

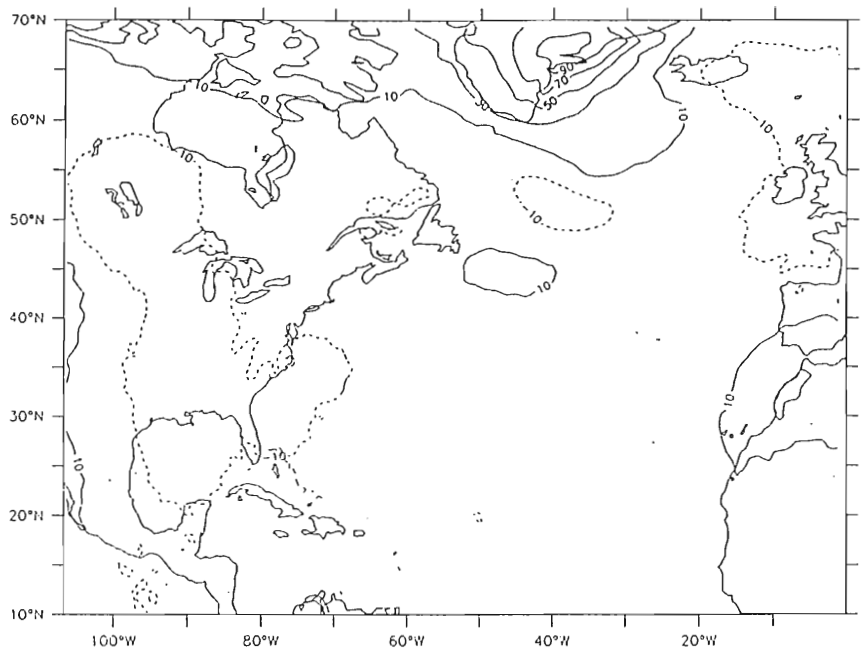

Fig. 5-3c: Same as fig. 5-3a except at 72 hours (9/00Z).

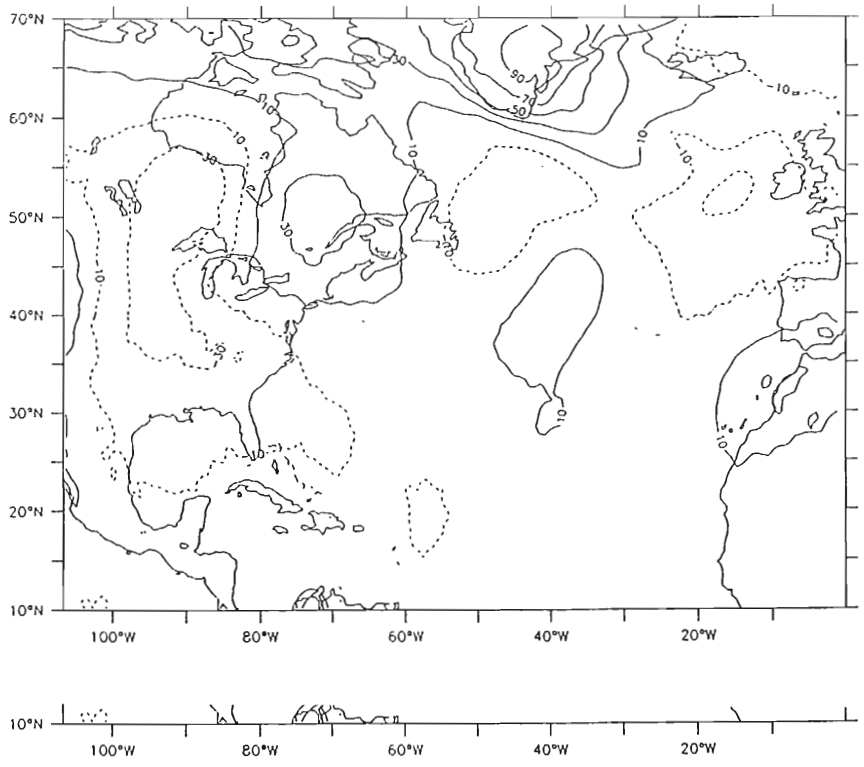

Fig. 5-3d: Same as fig. 5-3a except at 96 hours (10/00Z).

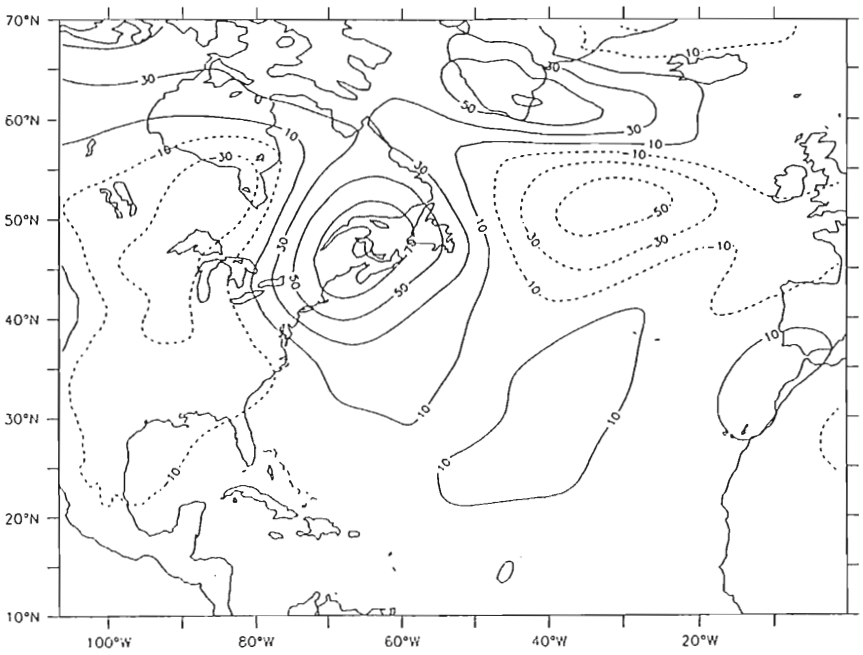

Fig. 5-3e: Same as fig. 5-3a except at 120 hours (11/00Z).

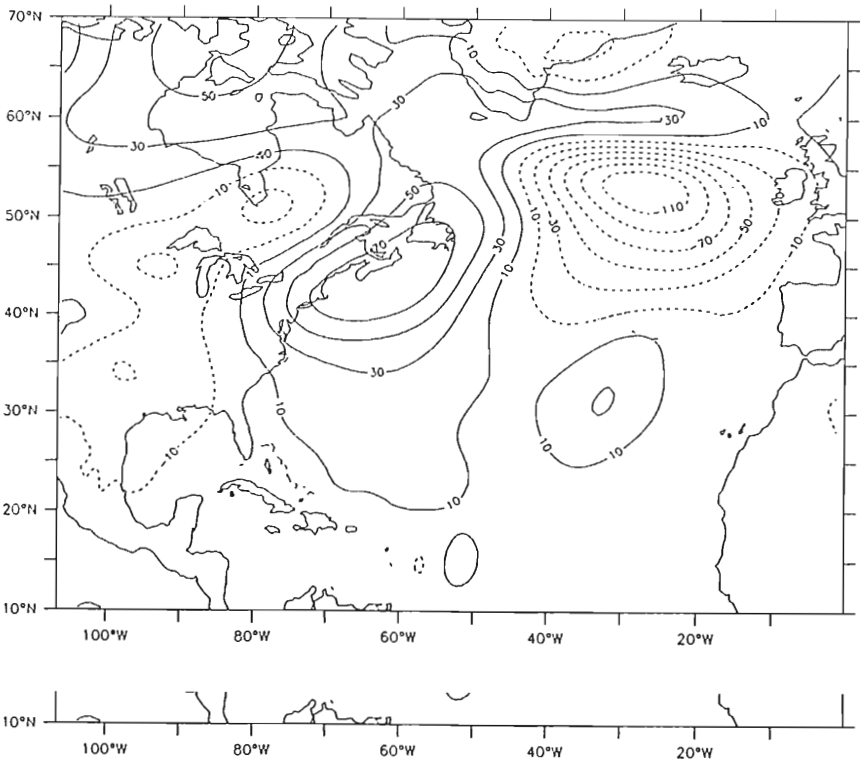

Fig. 5-3f: Same as fig. 5-3a except at 144 hours (12/00Z).

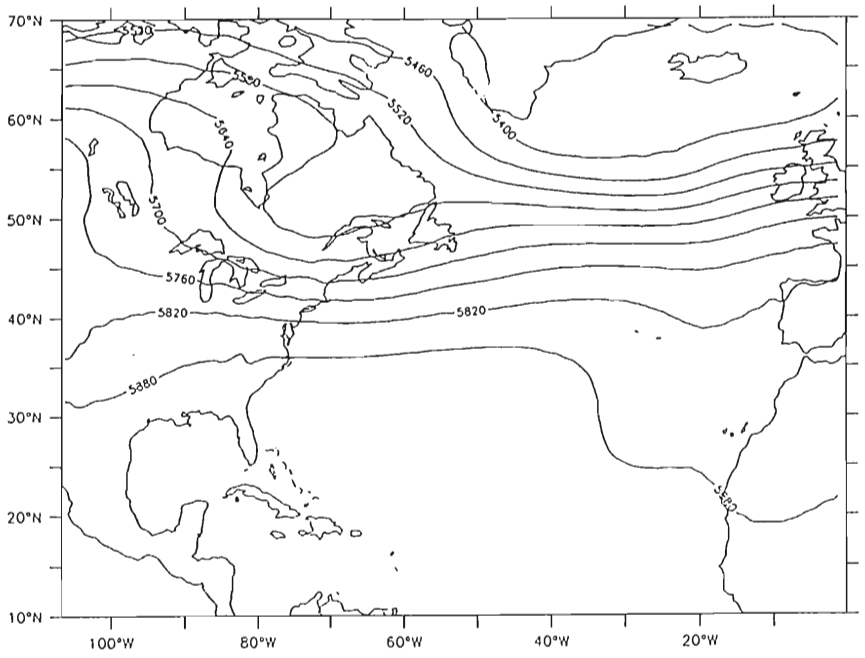

Fig. 5-4a: The 500 mb height contours for Case A at 144 hours (12/00Z) over the Northern Pacific Ocean (meters)

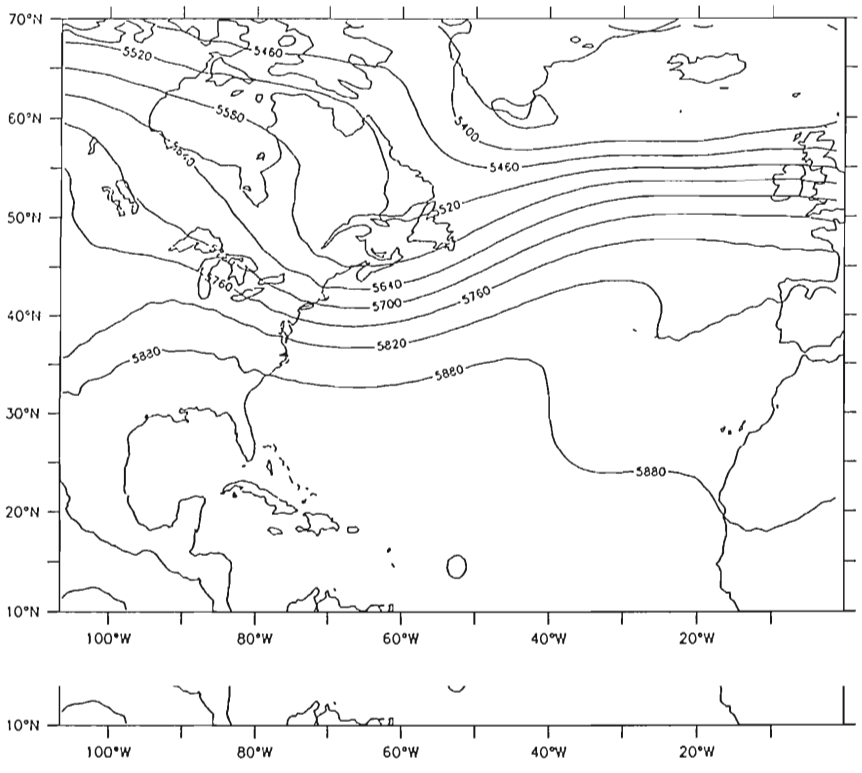

Fig. 5-4b: Same as fig. 5-4a except for Case B.

Figure 5-5 illustrates the 500 mb geopotential height difference field between Cases A and B over the Western Pacific Ocean as it evolves over the 6-day period. Two significant features develop in the difference field. They each correspond to the typhoons that develop during the period and reach a maximum geopotential height difference of minus 90 meters over Gerald and 250 meters over Holly-Freda. Figure 5-6 shows the sea level pressure (SLP) field from Case A as it develops over the 6-day period over the Western Pacific Ocean. Typhoon Gerald tracks toward China, but develops a split structure in its SLP field as it moves toward landfall at day 4. The overall track agrees well with the observed track in Fig. 5-7 from Krishnamurti et al. (1993). Freda and Holly develop and merge by day 4 and reach maximum intensity at day 5. Figure 5-8 shows the same SLP field for Case B. Gerald tracks westward and passes over land on day 4. The movement of Gerald in our two cases are closer to the observed track than the nudging case from Krishnamurti et al., but the intensities are poorly modeled. The timing of Gerald's movement and the intensity of the typhoon is better in Case A with the fine resolution SST. It is very close to that of the observed track seen in Fig. 5-7. Case B has Gerald making landfall one day faster than observed and continuing to intensify after moving over land. Freda and Holly develop as weak storms and gradually merge by day 6 in Case B in stark contrast to the robust development seen in Fig. 5-6 for Case A after they merge. The presence of the higher wavenumbers in the SST field has clearly benefited typhoon formation.

formation.

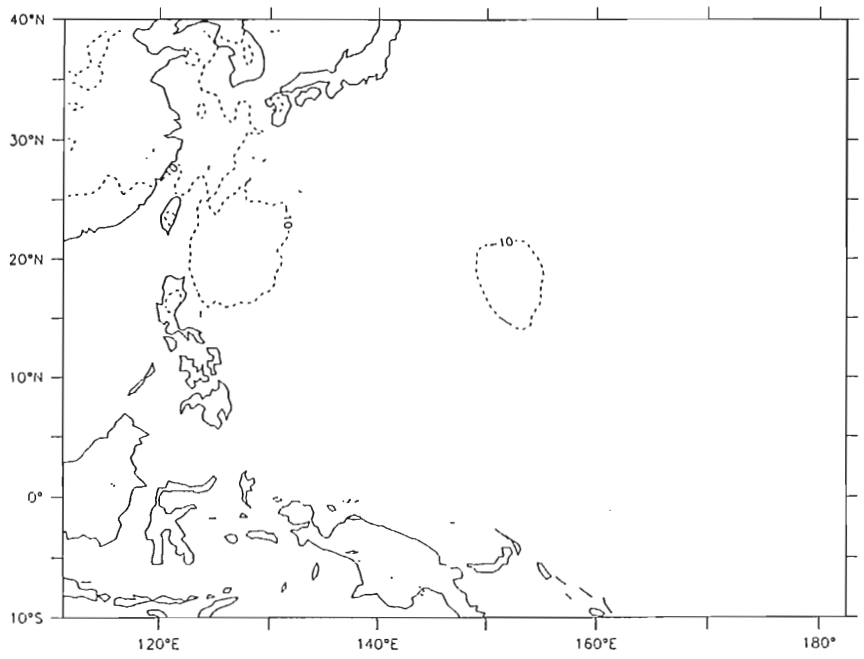

Fig. 5-5a: The 500 mb height differences after 24 hours of integration (7 September at 00Z) between Case A and Case B over the Western Pacific Ocean (meters).

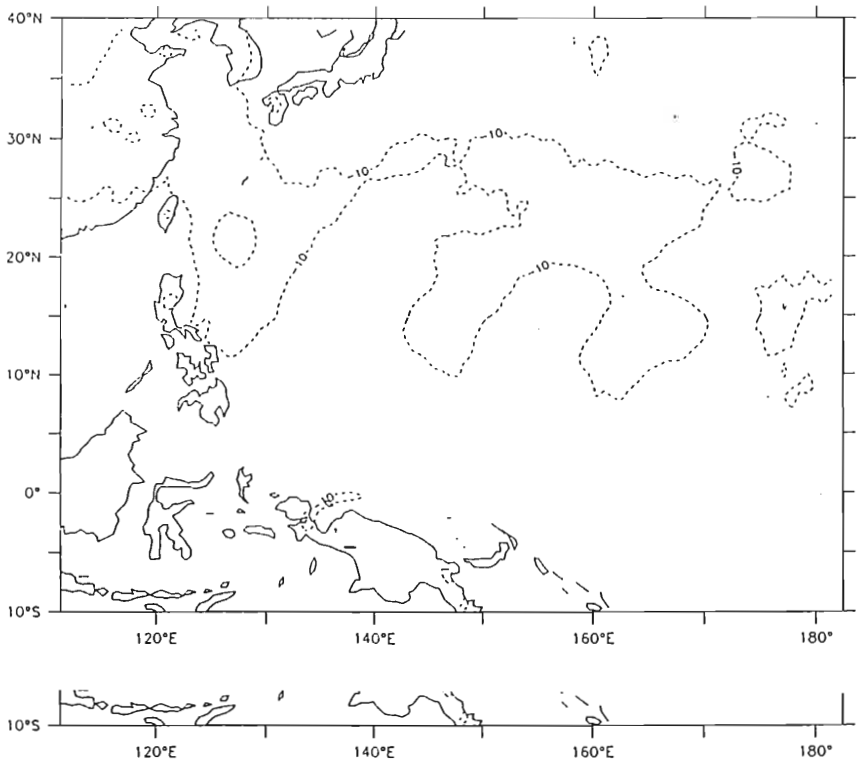

Fig. 5-5b: Same as fig. 5-5a except at 48 hours (8/00Z).

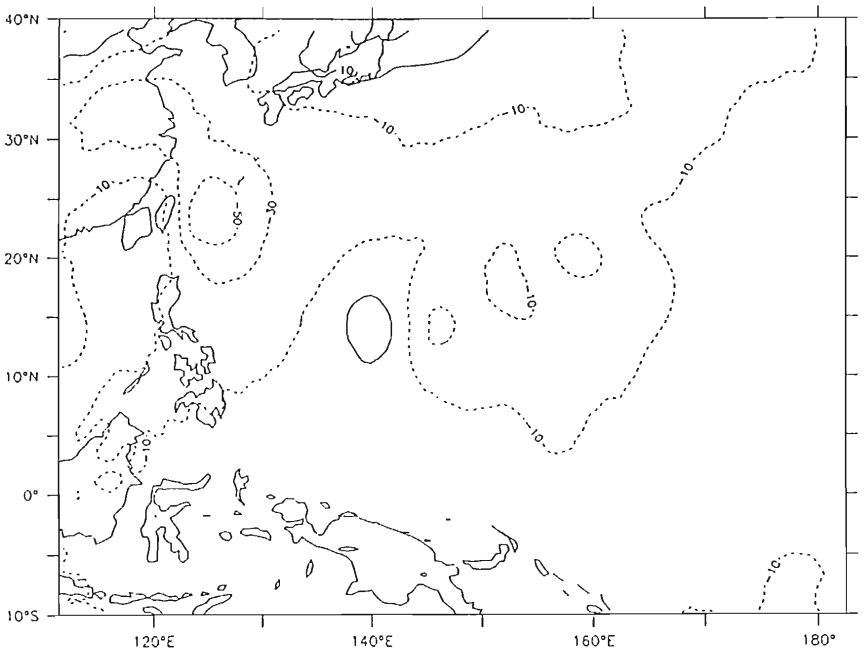

Fig. 5-5c: Same as fig. 5-5a except at 72 hours (9/00Z).

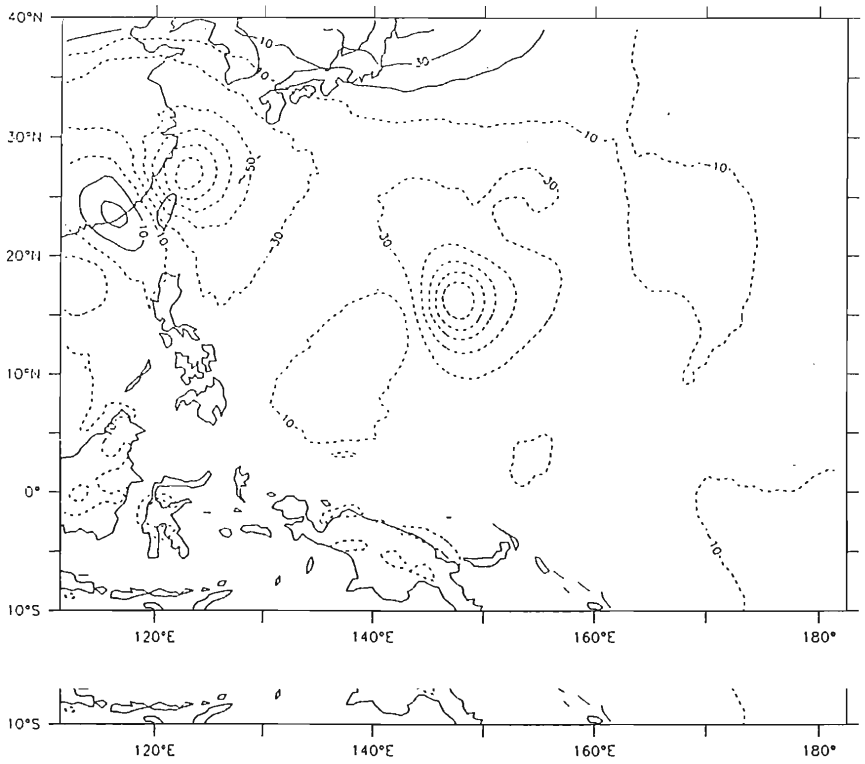

Fig. 5-5d: Same as fig. 5-5a except at 96 hours (10/00Z).

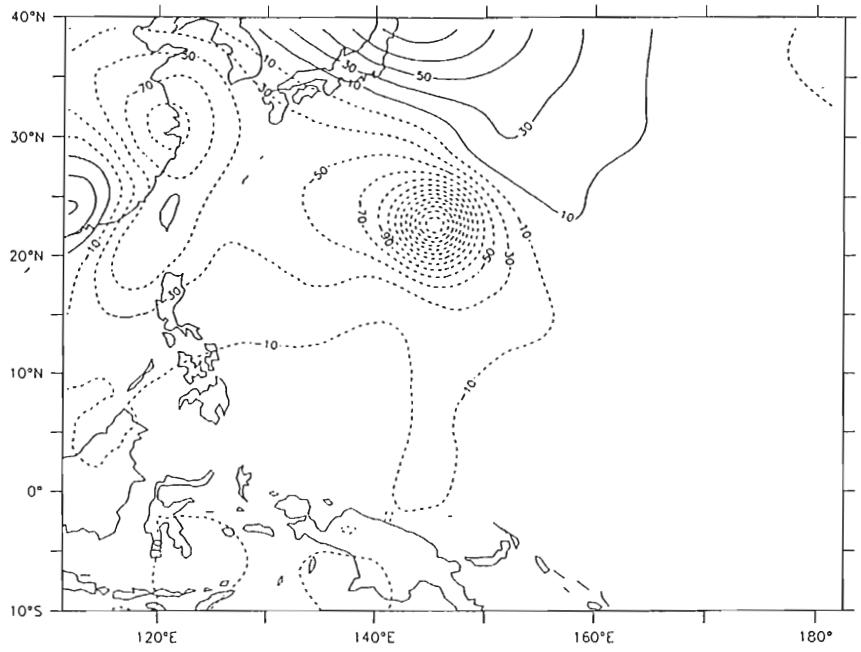

Fig. 5-5e: Same as fig. 5-5a except at 120 hours (11/00Z).

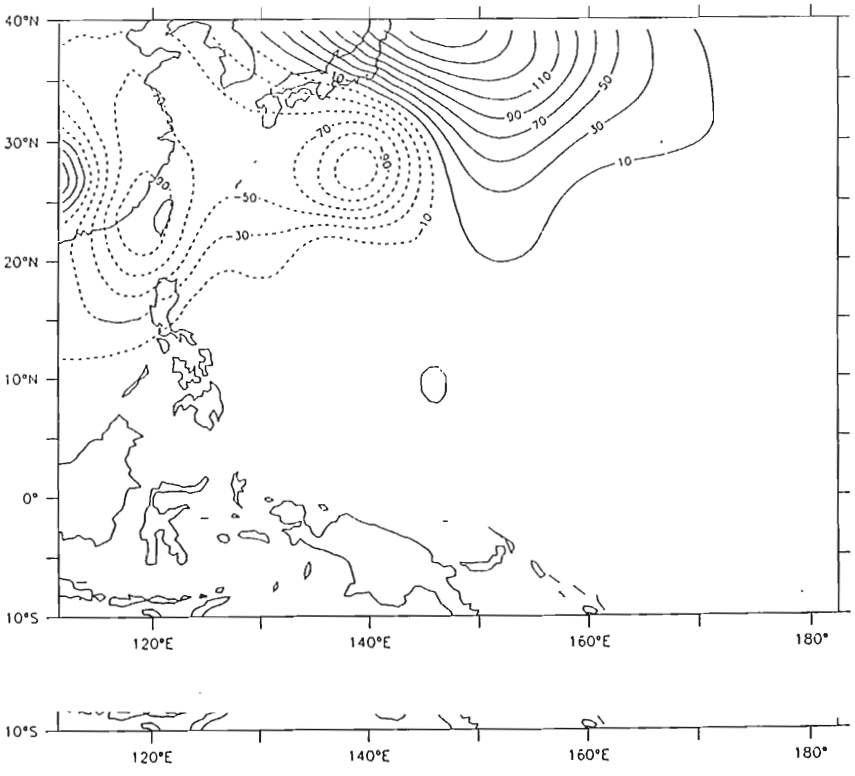

Fig. 5-5f: Same as fig. 5-5a except at 144 hours (12/00Z).

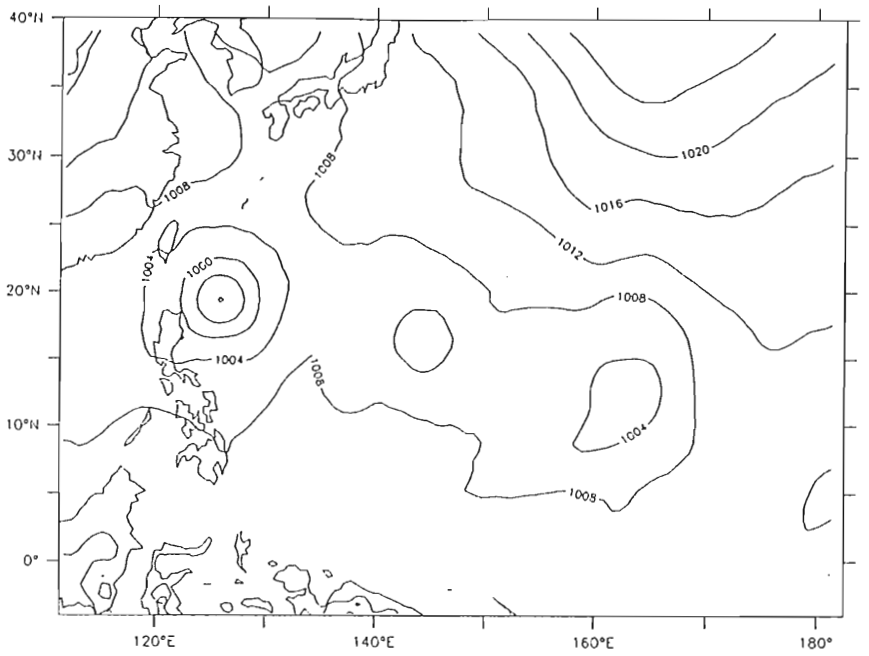

Fig. 5-6a: Sea level pressure at 24 hours (7/00Z) for Case A over the Western Pacific Ocean (millibars).

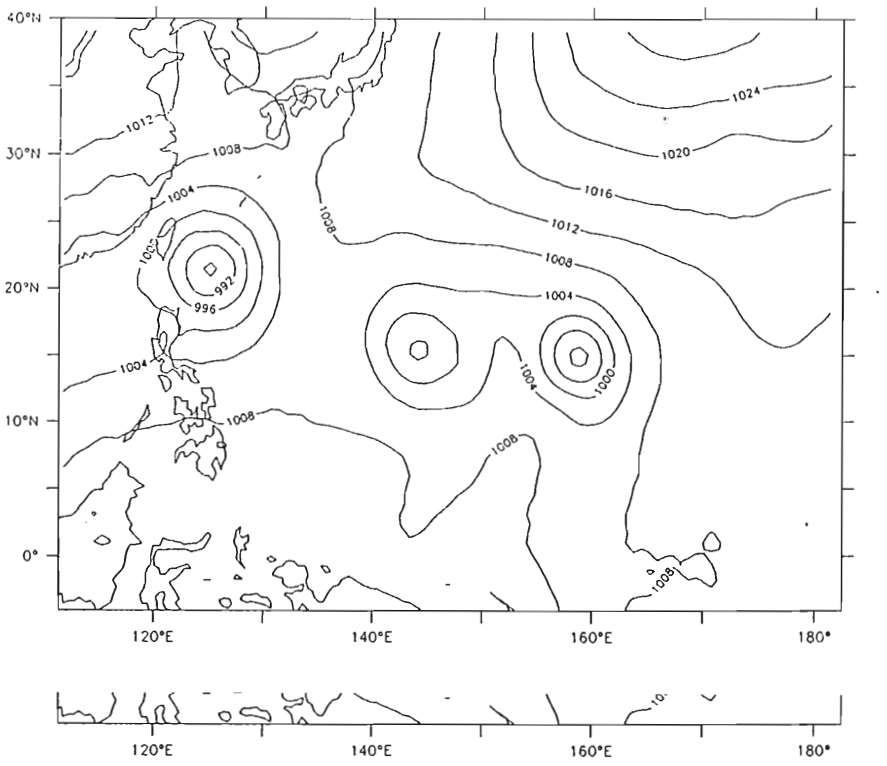

Fig. 5-6b: Same as fig. 5-6a except at 48 hours (8/00Z).

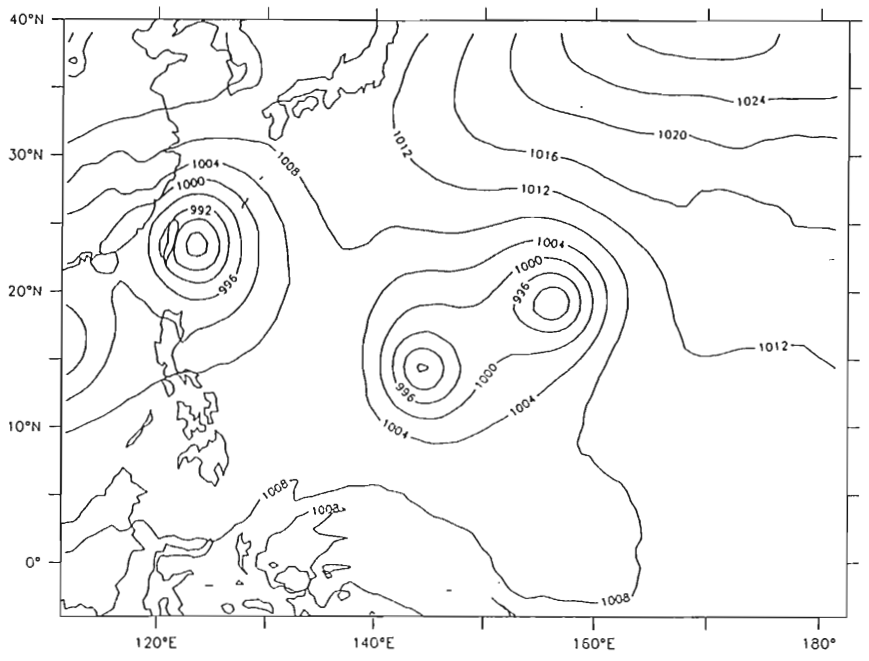

Fig. 5-6c: Same as fig. 5-6a except at 72 hours (9/00Z).

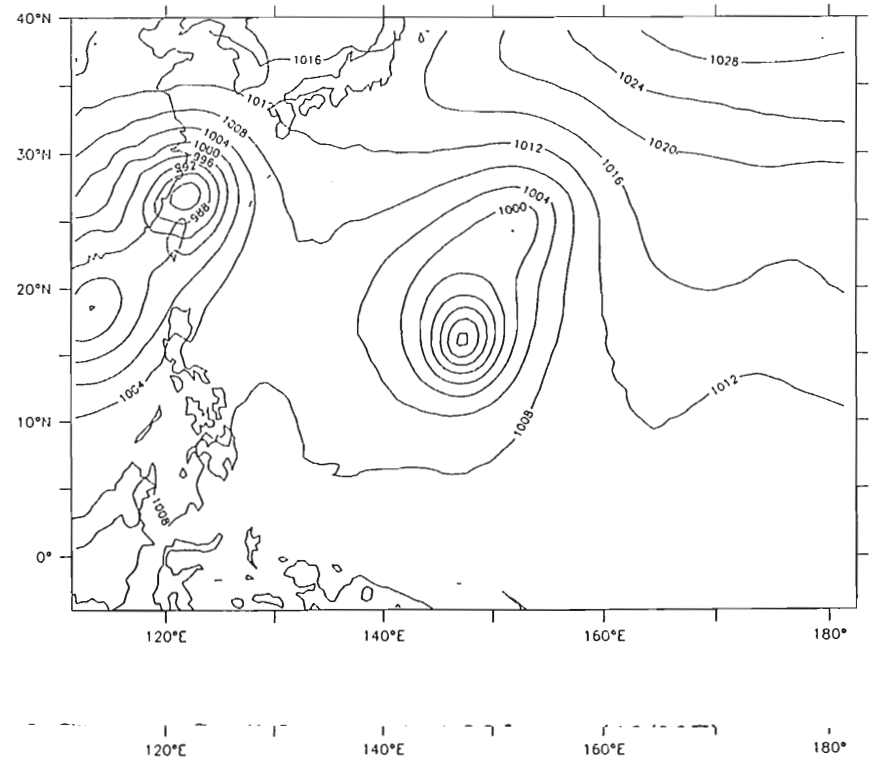

Fig. 5-6d: Same as fig. 5-6a except at 96 hours (10/00Z).

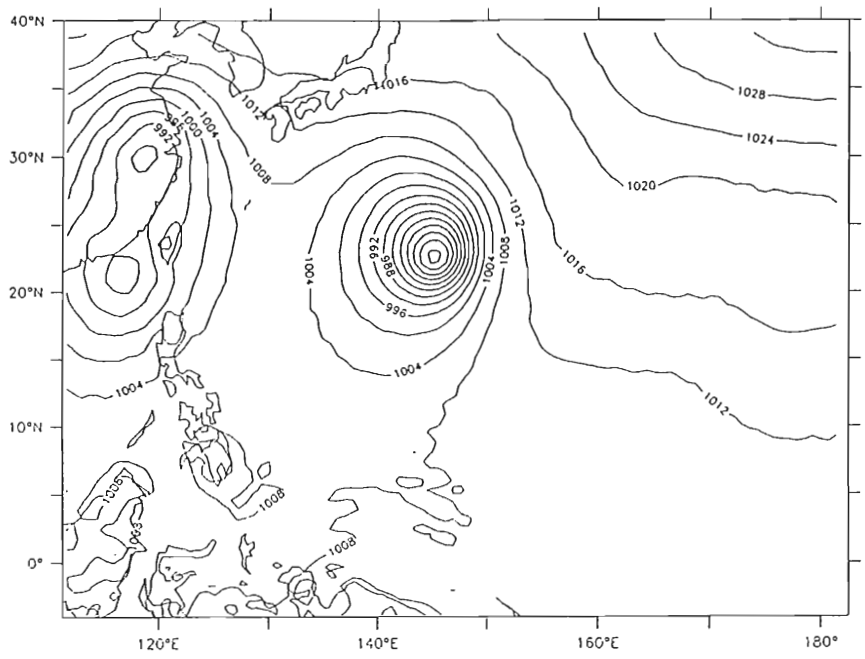

Fig. 5-6e: Same as fig. 5-6a except at 120 hours (11/00Z).

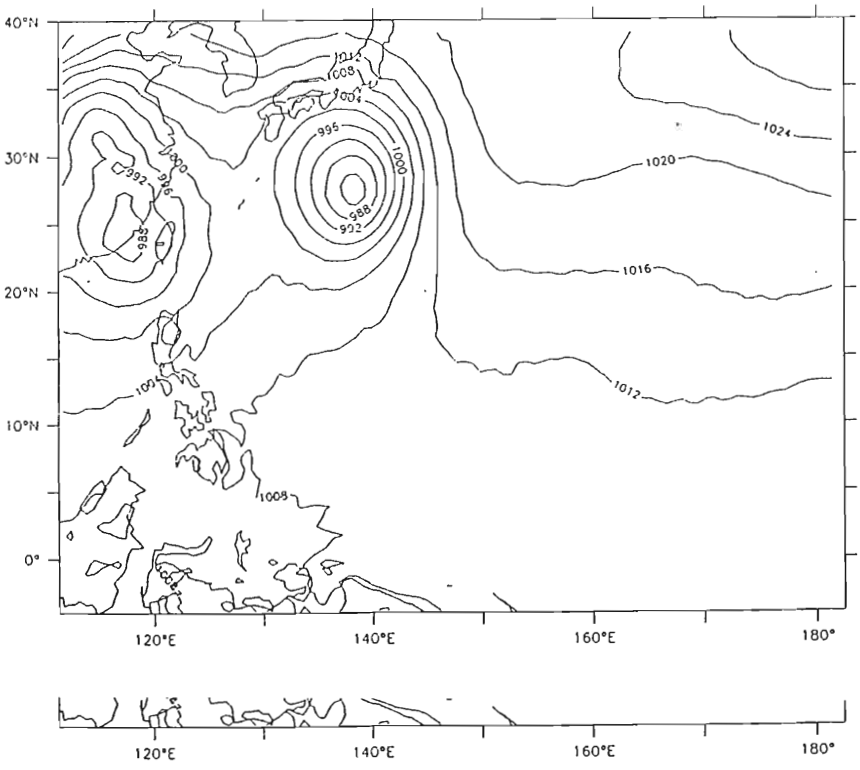

Fig. 5-6f: Same as fig. 5-6a except at 144 hours (12/00Z)..

. ____ Observed storm track
+ _ _ Case A storm track
o ----- Case B storm track

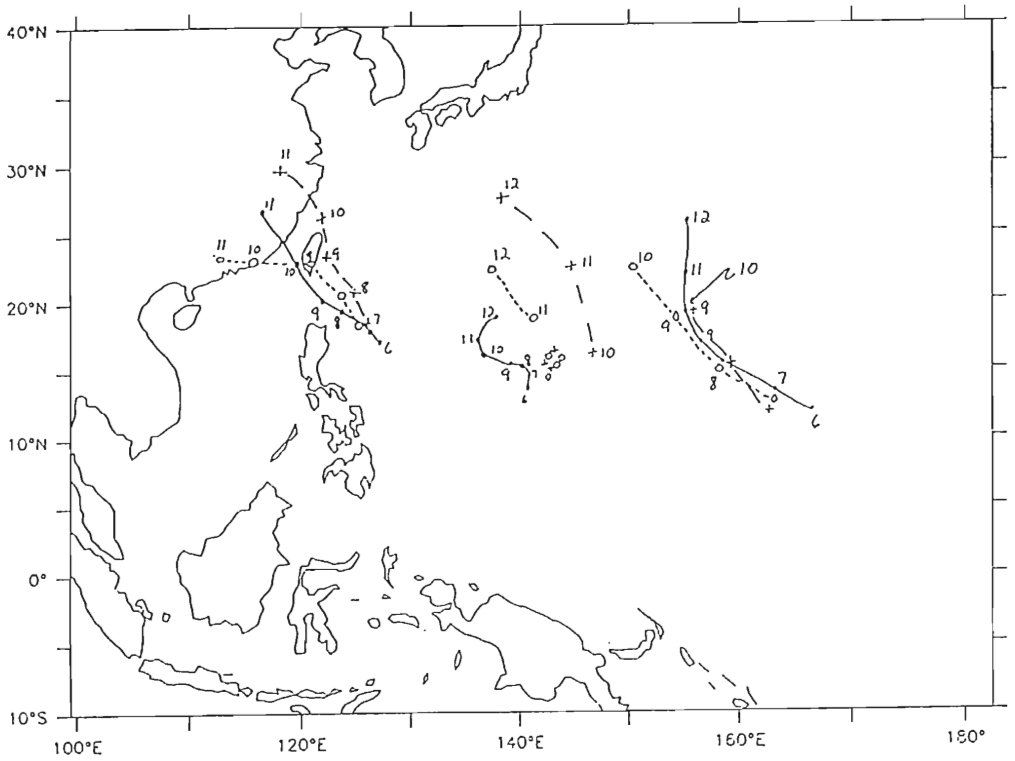

Fig. 5-7: Comparison of the Case A and Case B model storm tracks with the observed storm tracks.

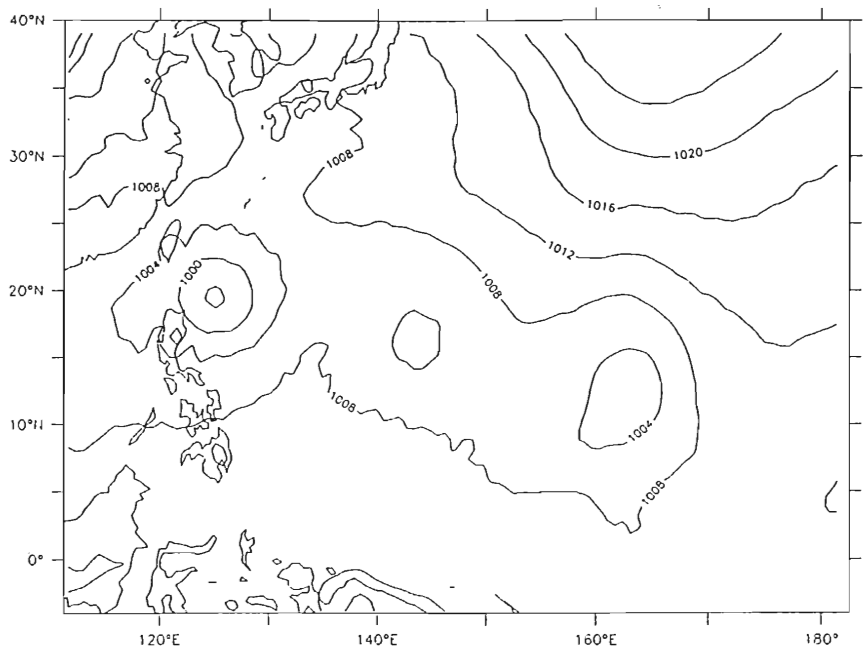

Fig. 5-8a: Sea level pressure from at 24 hours (7/00Z) for Case B over the Western Pacific Ocean (millibars).

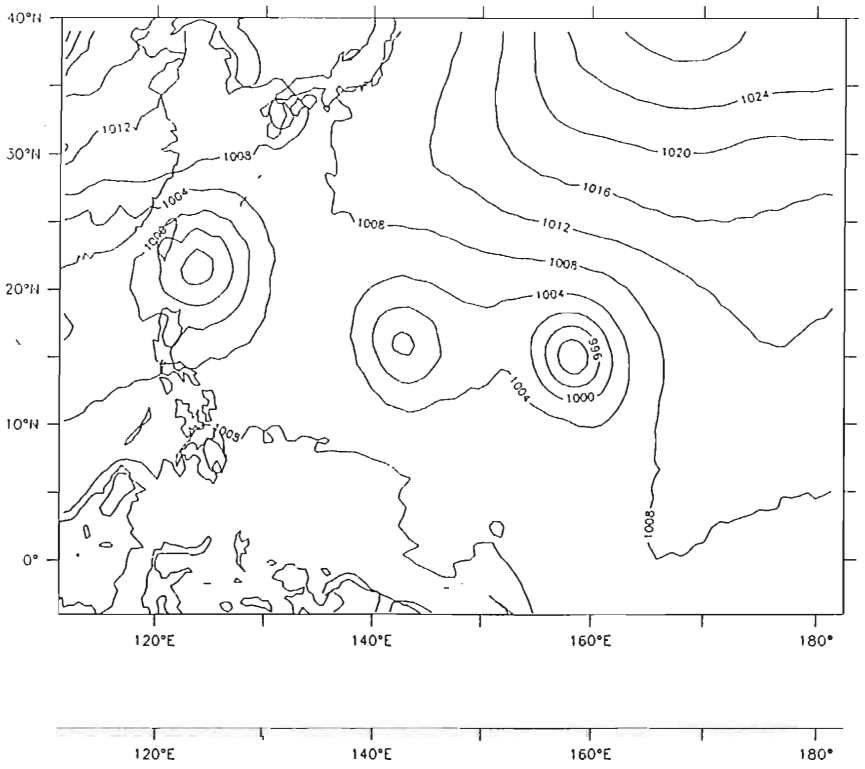

Fig. 5-8b: Same as fig. 5-8a except at 48 hours (8/00Z).

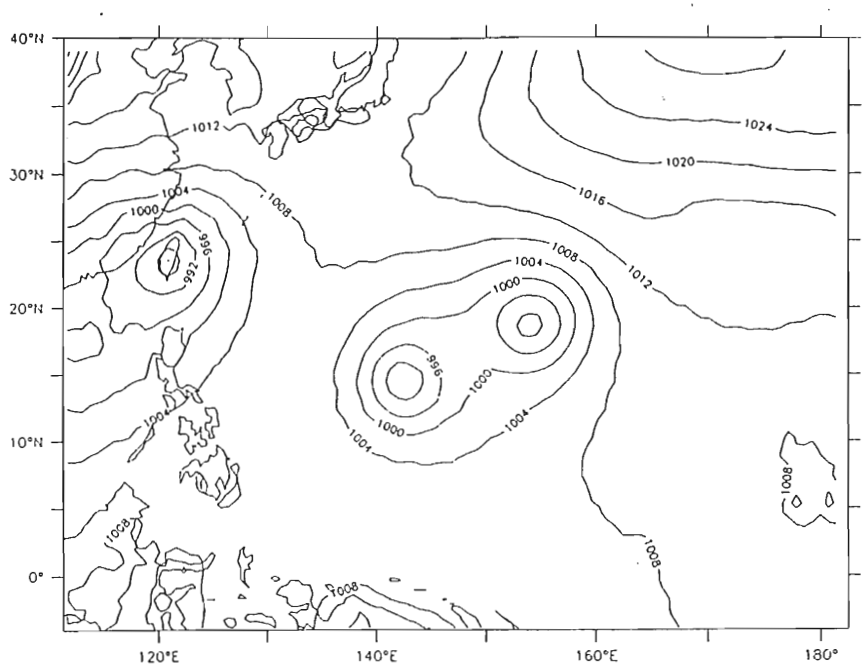

Fig. 5-8c: Same as fig. 5-8a except at 72 hours (9/00Z).

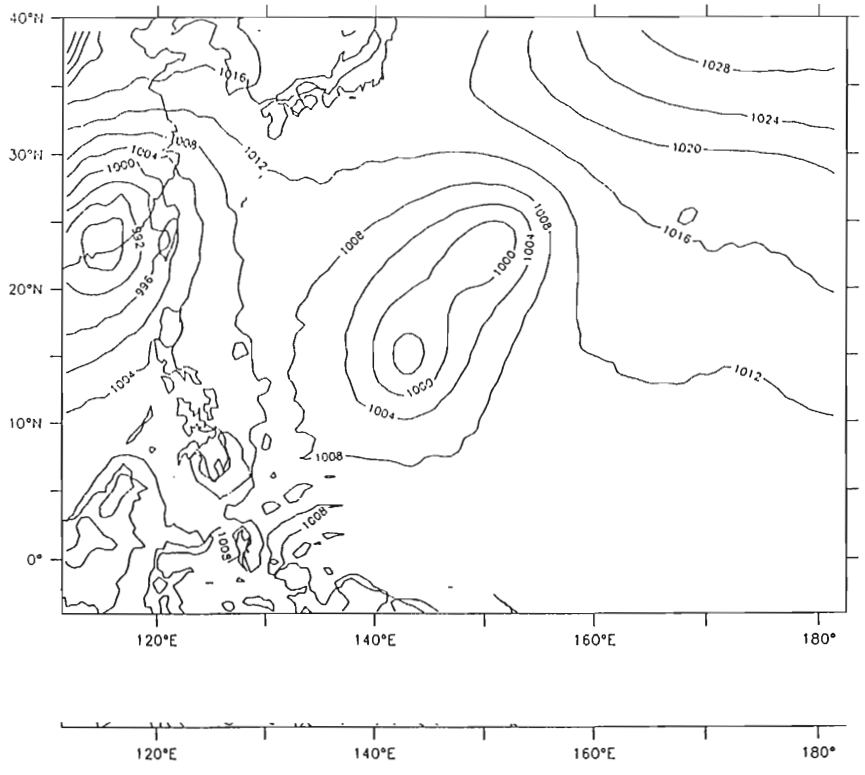

Fig. 5-8d: Same as fig. 5-8a except at 96 hours (10/00Z).

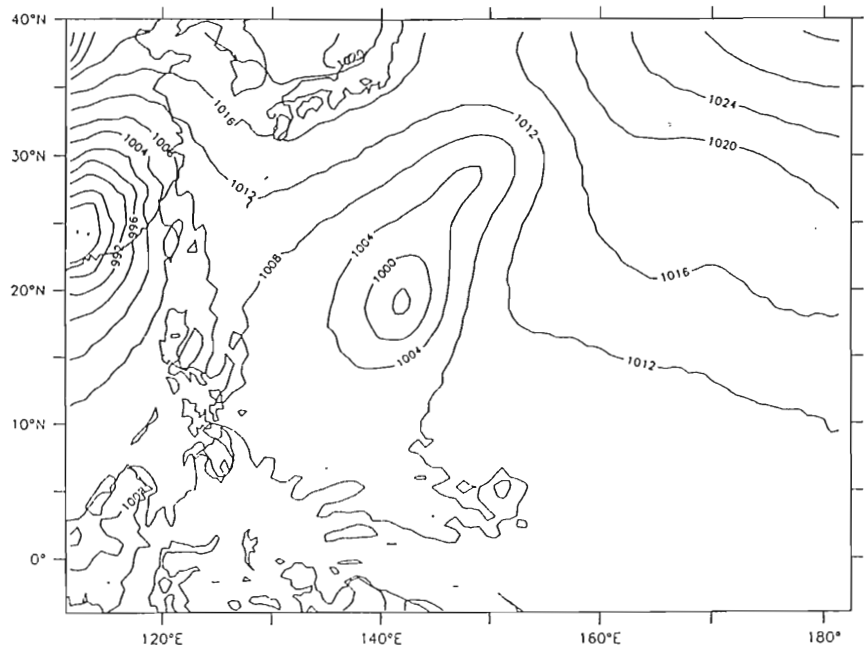

Fig. 5-8e: Same as fig. 5-8a except at 120 hours (11/00Z).

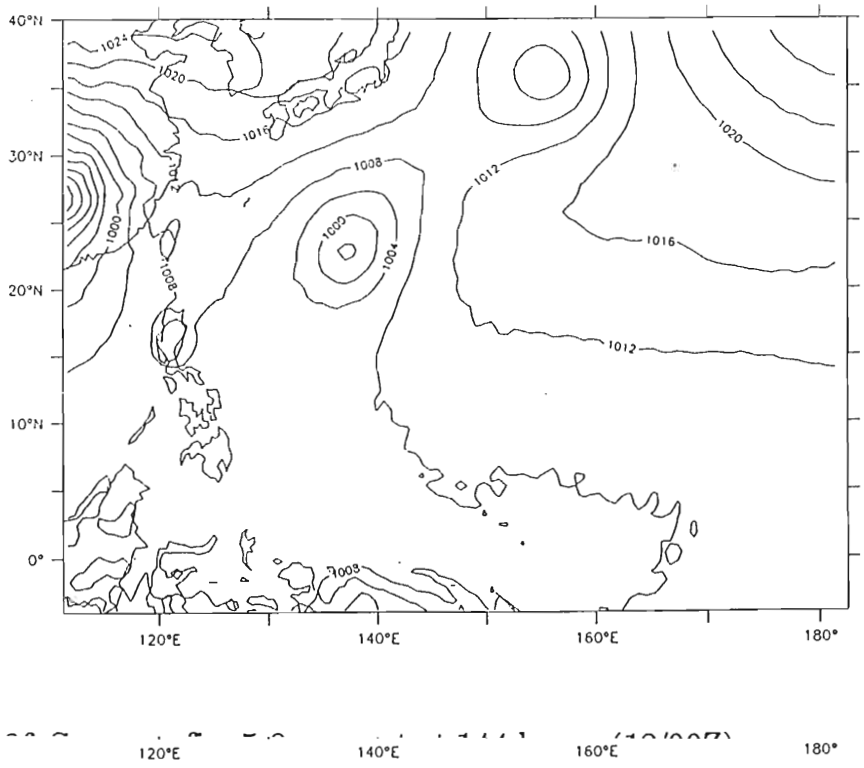

Fig. 5-8f: Same as fig. 5-8a except at 144 hours (12/00Z).

Figures 5-9 and 5-10 show the geopotential height difference fields between Cases A and C and Cases B and C respectively over the north Pacific at 8/00Z. Case C shows a height rise of 30-50 meters over the Rocky Mountains compared to Case B, which corresponds well with the 30-50 meters seen in Fig. 5-1 at the 8/00Z point. Similarities are also evident over Eastern China, Alaska and Siberia, although these are not dramatic at the 48 hour point in the model run. Overall, Case C looks to be much closer to Case A than to Case B at this point. Thus, the high wavenumbers from the patch covering Kuroshio have significantly affected the model output in this region.

Figures 5-11 and 5-12 show the geopotential height difference fields between Cases A and C and Cases B and C respectively over the north Atlantic. Here the difference fields are very similar, with the exception of the 70 meter negative height difference over Greenland in Fig. 5-12. This is very similar to the height difference in Fig. 5-2 at 8/00Z between Cases A and C.

Figures 5-13 and 5-14 show the geopotential height difference fields between Cases A and D and Cases B and D respectively over the north Pacific at 8/00Z. Differences in the model output by starting 12 hours earlier are evident here, but similarities with the results from Cases A and B can be drawn. Again we see a 50 meter difference over the Rocky Mountains as in Fig. 5-1 at 8/00Z. Figures 5-15 and 5-16 show the geopotential height difference fields between Cases A and D and Cases B and D respectively over the North Atlantic at 8/00Z. Again the difference fields are very similar, with the largest differences being over Greenland

and D respectively over the North Atlantic at 8/00Z. Again the difference fields are very similar, with the largest differences being over Greenland

as in Fig. 5-3 at 8/00Z and over Ireland and where similarities between

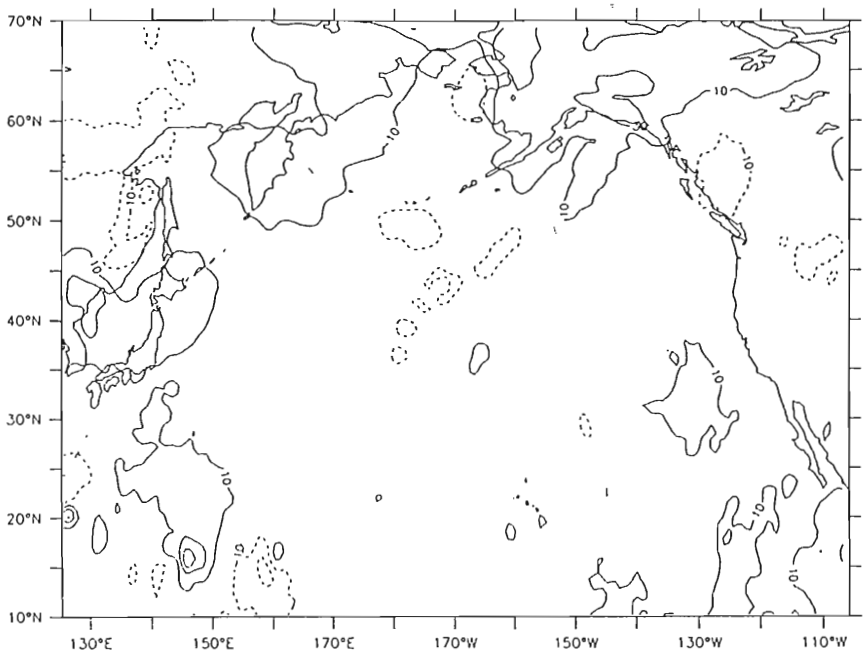

Fig. 5-9: The 500 mb height differences at 48 hours (8/00Z) between Case A and Case C over the Northern Pacific Ocean (meters).

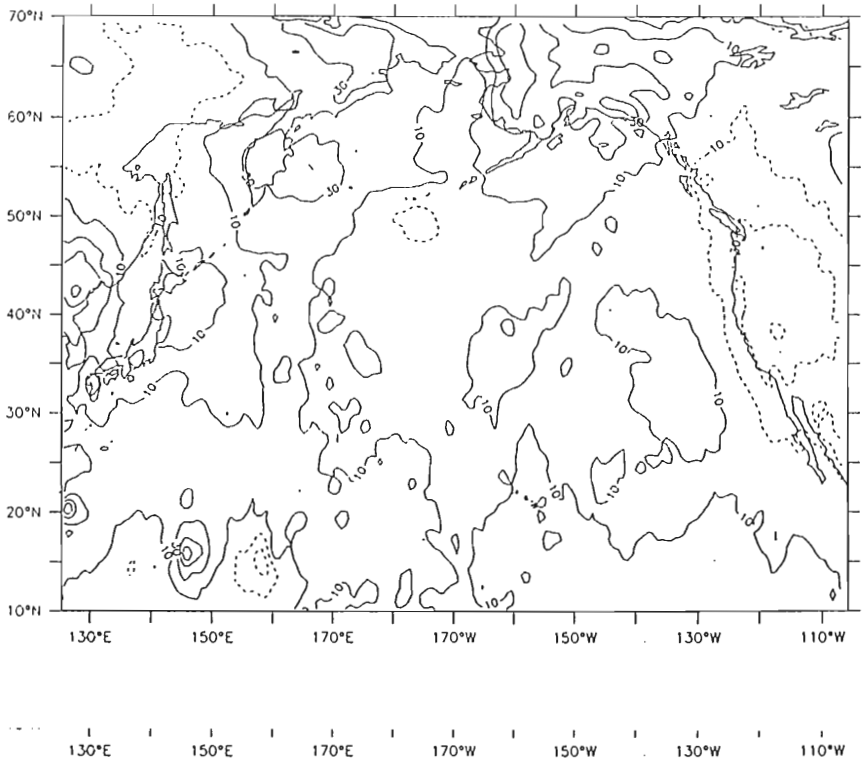

Fig. 5-10: The 500 mb height differences from 8/00Z between Case B and Case C over the Northern Pacific Ocean (meters).

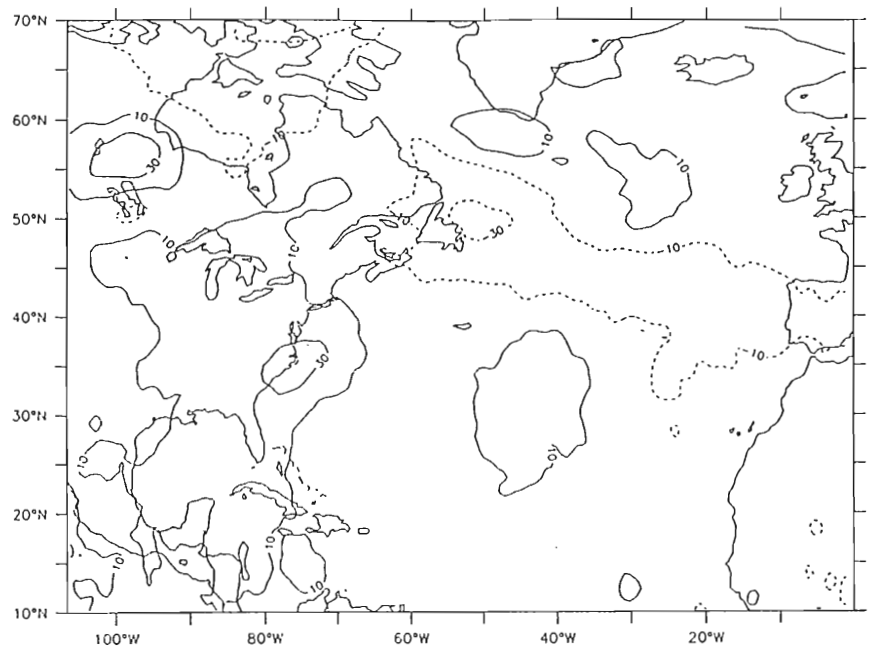

Fig. 5-11: The 500 mb height differences from 8/00Z between Case A and Case C over the Northern Atlantic Ocean (meters).

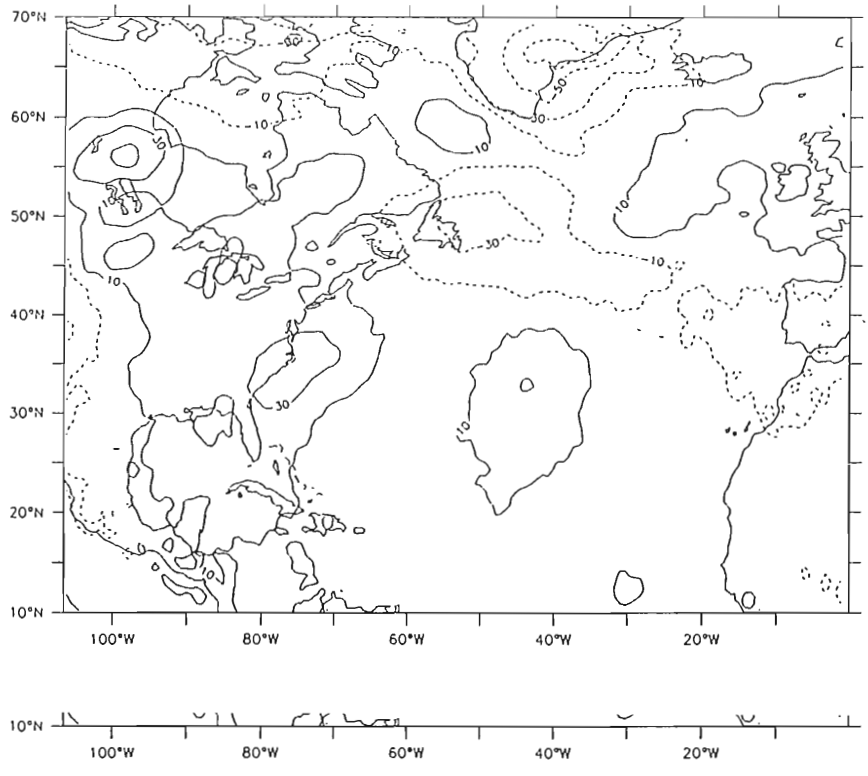

Fig. 5-12: The 500 mb height differences from 8/00Z between Case B and Case C over the Northern Atlantic Ocean (meters).

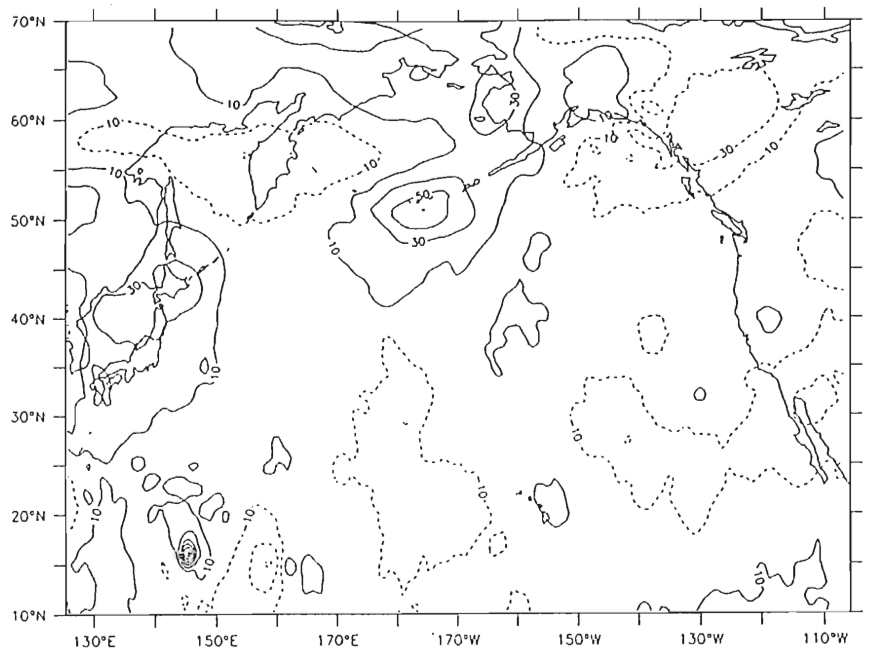

Fig. 5-13: The 500 mb height differences from 8/00Z between Case A and Case D over the Northern Pacific Ocean (meters).

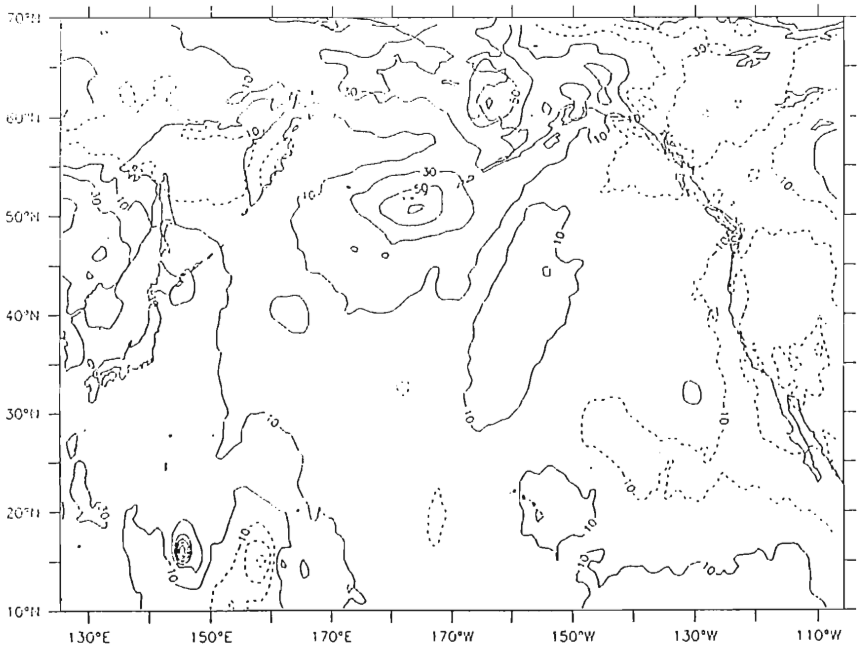

Fig. 5-14: The 500 mb height differences from 8/00Z between Case B and Case D over the Northern Pacific Ocean (meters).

Fig. 5-14: The 500 mb height differences from 8/00Z between Case B and Case D over the Northern Pacific Ocean (meters).

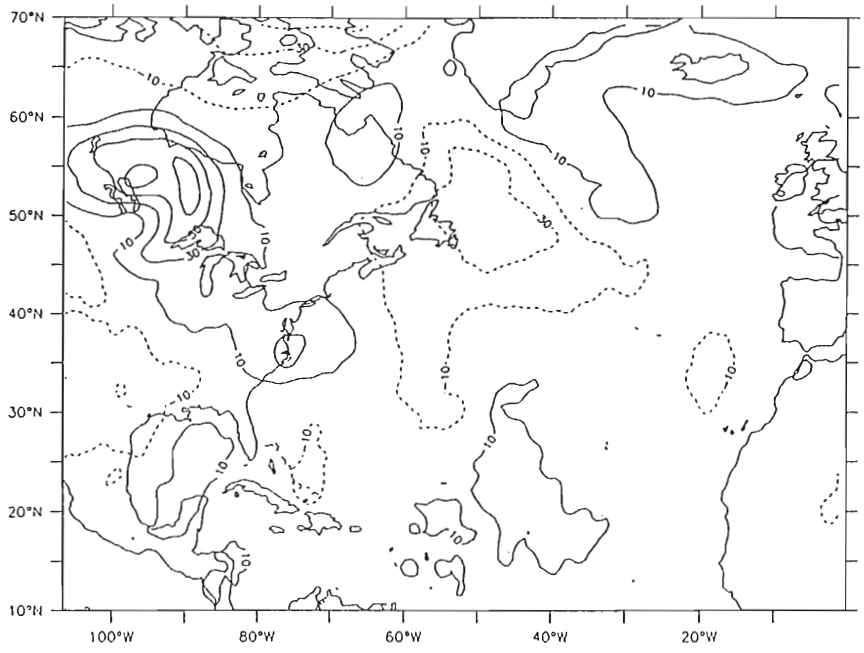

Fig. 5-15: The 500 mb height differences from 8/00Z between Case A and Case D over the Northern Atlantic Ocean (meters).

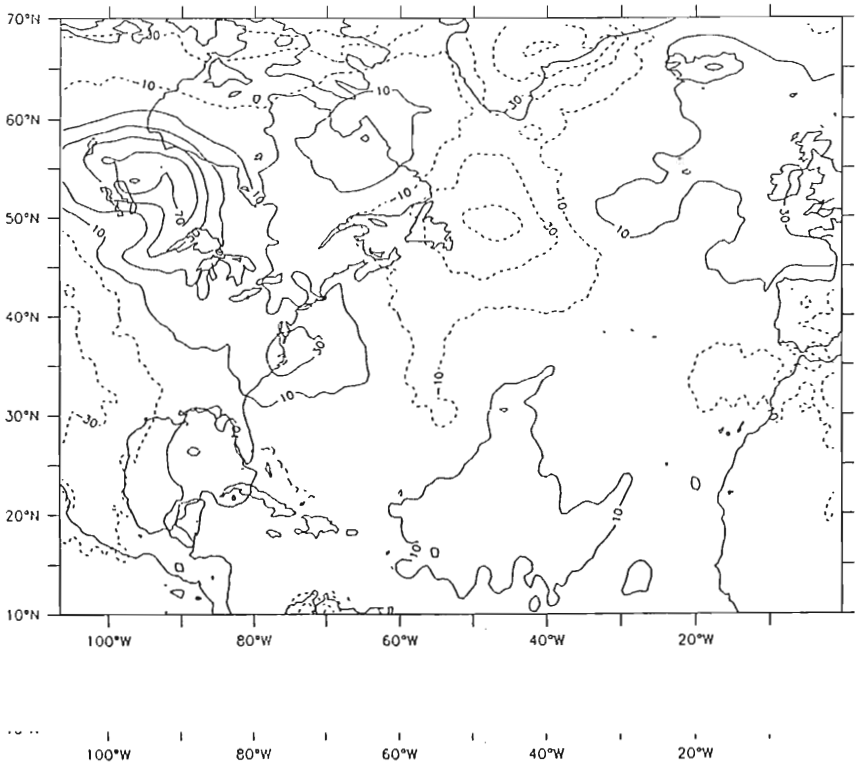

Fig. 5-16: The 500 mb height differences from 8/00Z between Case B and Case D over the Northern Atlantic Ocean (meters).

Figure 5-16 and Fig. 5-3 can be seen. The same features seen in Fig. 5-1 and Fig. 5-3 at 8/00Z are evident in Fig. 5-13 through Fig. 5-16.

Looking at the output from Cases A and B by examining the sum of the differences in the height fields provides an interesting look at how the forecasts diverge over the Northern Pacific and the Northern Atlantic Oceans. Figure 5-17 compares the root mean square differences (RMSD) in the geopotential heights at 500 mb for the two regions. The RMSD grow about the same for the two regions until about the 72 hour point when the RMSD over the Northern Pacific growth rate increases and the Northern Atlantic RMSD growth rate slows..

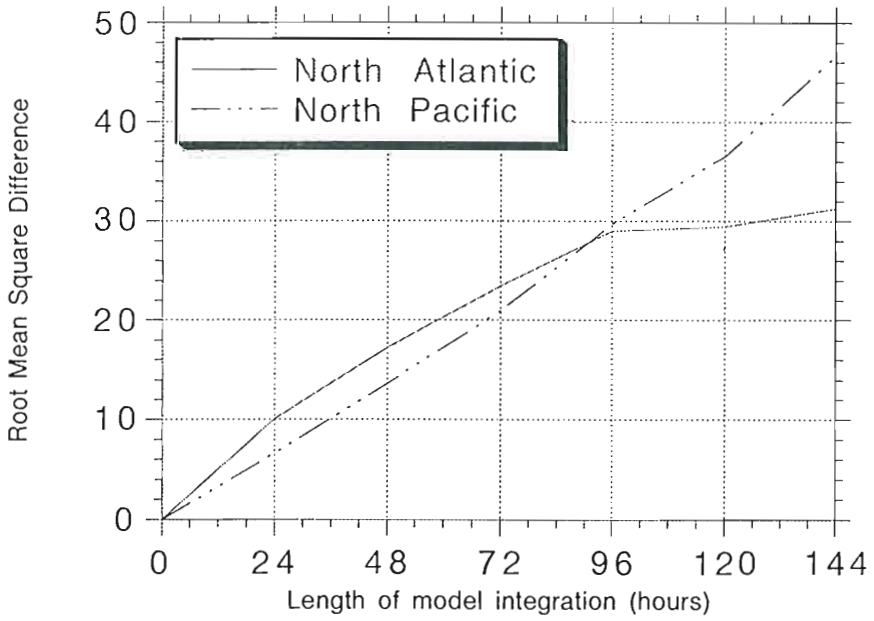

Fig. 5-17: Root mean square difference between Case A and Case B over the North Pacific and North Atlantic Oceans.

Fig. 5-17: Root mean square difference between Case A and Case B over the North Pacific and North Atlantic Oceans.

CHAPTER 6

CONCLUSIONS AND DISCUSSION

The results from this study demonstrate the importance of the higher wavenumbers in the SST field on the output from a high resolution atmospheric model. The differences that occur over and downstream from areas of high SST gradient, such as the Kuroshio, between Case A and Case B are shown to occur as a result of the difference in the boundary forcing SST. The similarities in the output among Cases A, C and D when compared to case B provide ample support for this conclusion.

Examination of the phase and amplitude relationships from the 500 mb height contours at 144 hours in Fig. 5-2a and Fig. 5-2b enables us to deduce the reasons for the differences between Cases A and B in Fig. 5-1f over the Northern Pacific.. The differences near Japan and over Siberia are directly attributable to the intensification of the combination typhoon in Case A which lowered the 500 mb heights south of Japan and induced ridging over Japan. This did not occur in Case B, thus the trough extending south from Siberia and the Sea of Okhotsk is well defined in Case B, but not in Case A. The typhoon intensification in Case A appears to be due the higher wavenumbers in the SST field, which result in somewhat warmer SST over this region in Case A. The warmer SST provided more energy for the storm development through latent and

somewhat warmer SST over this region in Case A. The warmer SST provided more energy for the storm development through latent and

sensible heat flux, intensified the storm which caused the 500 mb heights to be lower in Case A.

The features over the Northern Pacific are in good phase agreement with the trough extending southward from the Gulf of Alaska very similar in position and strength for the two cases. The trough is slightly stronger over Alaska which is a result of the change in the longwave pattern caused by the intensity of the typhoon south of Japan in Case A.

A similar analysis over the Northern Atlantic can be made using Figs. 5-3f, 5-4a and 5-4b. The differences over the Hudson Bay and Newfoundland in Fig. 5-3f are directly attributable to the phase difference between Case A and B over this region. The differences over the Northeast Atlantic are due to a slight difference in the longwave pattern. We believe that the phase difference results from the downstream effects of the Kuroshio region on the longwave pattern. The effects of the high spatial SST gradient over the Gulf Stream are not as easily traced. We feel that this is because there were no weather systems active over the region during the forecast period. We believe the Gulf Stream SST field had an impact on the longwave pattern and that a study with data from a period with a strong weather system over the Gulf Stream would yield downstream effects as prominent as those seen from the Kuroshio region in this study. The stronger development of the typhoon in the Kuroshio region for Case A has directly impacted the growth of the RMSD in Fig. 5-17 over the Pacific, whereas the RMSD growth is slower in the Atlantic where no strong feature exists.

Prominent features in the comparisons between Cases A, C and D where no strong feature exists.

Prominent features in the comparisons between Cases A, C and D and Case B are the strong differences over Greenland and the Rocky

Mountains at the 48 hour point. We can only speculate that downstream effects from the Kuroshio SST field on the longwave pattern were responsible for these features. Another case study would be necessary to conclude that these features are definitely a result of the higher wavenumbers in the SST spectrum.

The Case D results show that the model is not perfect, but the differences between Case B and Case D are where we expected them in that they concur with the Case A, Case B differences. Thus, the models response to the initial state of the atmosphere did not result in the differences seen between Cases A and B.

The rapid growth in the difference fields between Case A and Case B after the first 48 hours of integration suggests that the effects of the SST data on the model output become stronger as the model run progresses. The impact of the fine resolution SST on the development of the typhoons suggests that the higher wavenumbers are critical to the growth of the storms. The storms intensify faster over the ocean and lose strength over the land in Case A whereas in Case B typhoon Gerald intensifies after moving over land. The availability of good high resolution SST data makes it possible for at least weekly insertion of new SST fields into the model. The results of this study strongly suggest that the persistent application of the best SST would result in important improvements in the behavior of global atmospheric forecast models.

Previous studies have examined the effect of horizontal resolution by varying the resolution of the atmospheric model. This study is based solely on the spatial spectrum of the boundary forcing SST field. The difference

varying the resolution of the atmospheric model. This study is based solely on the spatial spectrum of the boundary forcing SST field. The difference

in approach results in several conclusions on how the ocean boundary

forcing resolution will effect the response of an atmospheric model. The higher wavenumbers in the SST are responsible for important differences in model output. The principal areas affected are conclusively demonstrated to be directly downstream from or adjacent to areas of high gradient in the SST field such as near oceanic western boundary currents where the variance in the higher wavenumbers forms a significant part of the spectrum.

Other studies have used model forecast SST fields at T21 and T42 truncation or climatological SST data. Since the observed SST data have much more variance in the higher wavenumbers than climatological SST data, the effects of the higher wavenumbers are poorly modeled using climatological SST data. Using the data from a T21 or T42 ocean model to force the model would also result in the loss of a significant portion of the overall variance and is also a poor choice for good atmospheric models.

Comparison of the results from this study with other recent studies on the impact of horizontal resolution on model output, leads us to several conclusions about how SST data should be used in atmospheric modeling. The SST data should be carefully examined to ensure that important structures due to high wavenumbers are not omitted from the boundary forcing. Modelers might use a subgridscale heat flux parameterization similar to the cumulus parameterization schemes used in atmospheric models to include the effects of the higher wavenumbers in the SST field. The most recent SST data should be inserted frequently, perhaps weekly, into climate models using the high resolution data available from NMC and Miami/Rosensteil. Coupled air-ocean models should employ a high

into climate models using the high resolution data available from NMC and Miami/Rosensteil. Coupled air-ocean models should employ a high

resolution ocean to ensure that physical processes in the air-sea interaction

are not omitted. The ocean part of the model could be spun-up using the best SST data inserted weekly.

REFERENCES

Businger, J. A., J. C. Wyngard, Y. Izumi and E. F. Bradley, 1971: Flux profile relationship in the atmospheric surface layer. *J. Atmos. Sci.,* 28, 181-189.

Gleckler, J. P., K. E. Taylor, 1993: The effect of horizontal resolution on ocean surface heat fluxes in the ECMWF model. *Clim. Dynamics*, 9, 17-32.

Harshvardan and T. G. Corsetti, 1984: Longwave parameterization for the UCLA/GLAS GCM. NASA Tech. Memo. 86072, 52 pp.

Kanamitsu, M., J. C. Alpert, K. A. Campana, P. M. Caplan, D. G. Deaven, M. Irdell, B. Katz, H.-L. Pan, J. Sela and G. H. White, 1991: Recent changes implemented into the global forecast system at NMC. *Wea. Forecasting,* 6 425-435.

Kanamitsu, M., K. Tada, K. Kudo, N. Sato and S. Ita, 1983: Description of the JMA operational spectral model. *J. Meteor. Soc. Japan,* 61, 812-828.

Kanamitsu, M.,1975: On numerical prediction over a global tropical belt. Report No. 75-1, Department of Meteorology, The Florida State University, 1-282.

Kitade, T., 1983: Nonlinear normal mode initialization with physics. *Mon. Wea. Rev.,* 111, 2194-2213.

Krishnamurti, T. N., H. S. Bedi, D. Oosterhof and V. Hartiker, 1994: The formation of Hurricane Frederic of 1979. *Mon. Wea. Rev.*, 122, 1050-1074.

Krishnamurti, T. N., H. S. Bedi and K. Ingles, 1993: Physical Initialization using SSM/I rain rates. *Tellus*, 45A, 247-269.

Krishnamurti, T. N., J. Xue, H. S. Bedi, K. Ingles and D. Oosterhof, 1991: Physical Initialization for numerical weather prediction over the tropics. *Tellus*, 43AB,53-81.

Krishnamurti, T. N., S. Low-Nam and R. Pasch, 1983: Cumulus parameterization and rainfall rates II. *Mon. Wea. Rev.,* 111, 816-828.

Krishnamurti, T. N., S. Low-Nam and R. Pasch, 1983: Cumulus parameterization and rainfall rates II. *Mon. Wea. Rev.,* 111, 816-828.

Lacis, A. A. and J. E. Hansen, 1974: A parameterization of the absorption of solar radiation in the earth's atmosphere. *J. Atmos. Sci.,* 31, 118-133.

Louis, J. F., 1979: A parametric model of vertical eddy fluxes in the atmosphere. *Bound.-Layer Meteor.*, 17, 187-202.

Mo, K. C.,X. L. Wang and M. S. Tracton, 1994: Tropical and extratropical interaction and its impact on extended-range forecasting. Part I: The impact of sea surface temperature anomalies. *Mon. Wea. Rev.*, 122, 274-290.

Namias, J., 1974: Longevity of a coupled air-sea-continent system. *Mon. Wea. Rev.*, 102, 638-648.

Petersen, R. A., G. J. Dimego, J. E. Hoke, K. E. Mitchell and J. P. Gerrity, 1991: Changes to NMC's regional analysis and forecast system. *Wea. Forecasting*, 6, 133-141.

Reynolds, R. W. and T. M. Smith, 1994: Improved global sea surface temperature analyses using optimum interpolation. *J. Climate*, 7, 929-948.

Reynolds, R. W., 1991: A new global sea surface temperature analysis. *Technical Procedures Bulletin*, Number 393, Available from National Weather Service, Office of Meteorology, Silver Spring, MD 20910.

Reynolds, R. W., 1988: A real-time global sea surface temperature analysis. *J. Climate*, 1, 75-86.

Reynolds, R. W., 1978: Sea surface temperature anomalies in the North Pacific. *Tellus*, 30, 97-103.

Smith, E., 1992: A User's guide to the NOAA advanced very high resolution radiometer multichannel sea surface temperature data set. Available from Physical Oceanography Distributed Active Archive Center, Jet Propulsion Laboratory, California Institute of Technology, Pasadena, CA.

Tiedtke, M., 1984: The sensitivity of the time-mean large-scale flow to cumulus convection in the ECMWF model. *Workshop on Convection in Large-Scale Numerical Models,* Reading, UK, ECMWF, 297-316.

Trenberth, K. E., A. Solomon, 1993: Implications of global atmospheric spatial spectra for processing and displaying data. *J. Climate*, 6, 531-545?

Von Storch, H., D. Schriever, K. Arpe, G. W. Branstator, R. Legnani, U. Ulbrich, 1993: Numerical experiments on the atmospheric response to cold equatorial pacific conditions ("La Nina") during northern summer. Max-Planck-Institut für Meteorologie, Report No. 106. 22pp.

Ulbrich, 1993: Numerical experiments on the atmospheric response to cold equatorial pacific conditions ("La Nina") during northern summer. Max-Planck-Institut für Meteorologie, Report No. 106. 22pp.

Wallace, J. M., S. Tibaldi and A. J. Simmons, 1983: Reduction of systematic forecast errors in the ECMWF model. *Workshop on Convection in Large-Scale Numerical Models,* Reading, UK, ECMWF, 297-316.

Biographical Sketch

Brent Hickel was born in Williston ND on December 15, 1959, the second of four children to Dan and Mary Gail Hickel. He graduated from Capitol High School, Helena MT in June of 1978. He completed a bachelor of science degree in Chemical Engineering from Montana State University in June of 1982. He entered the United States Air Force in 1985 and was trained as weather officer at Texas A&M University in 1986. After tours of duty at Hill AFB, UT and Ramstein AB, Germany he began graduate work at the Florida State University in August of 1992. Upon completion of his graduate work Brent will be assigned to Los Angeles AFB, CA.